Published in Journal of Volcanology and Geothermal Research 227-228, 15-31, 2012
which should be used for any reference to this work

A geochemical and geophysical investigation of the hydrothermal complex of Masaya volcano, Nicaragua

Guillaume Mauri [a,*], Glyn Williams-Jones [a], Ginette Saracco [b], Jeffrey M. Zurek [a]

[a] Department of Earth Sciences, Simon Fraser University, Burnaby, BC, Canada
[b] CNRS-CREGE-UMR 7330, équipe de Modélisation,Université Aix-Marseille, Modélisation, Europole de l'Arbois, BP 80, 13545 Aix-en-Provence cedex 4, France

ABSTRACT

Masaya volcano, Nicaragua, is a persistently active volcano characterized by continuous passive degassing for more than 150 years through the open vent of Santiago crater. This study applies self-potential, soil CO_2 and ground temperature measurements to highlight the existence of uprising fluids associated to diffuse degassing structures throughout the volcano. The diffuse degassing areas are organized in a semi-circular pattern and coincide with several visible and inferred surface volcanic structures (cones, fissure vents) and likely consist of a network of buried faults and dykes that respectively channel uprising flow and act as barrier to gravitational groundwater flow. Water depths have been estimated by multi-scale wavelet tomography of the self-potential data using wavelets from the Poisson kernel family. Compared to previous water flow models, our water depth estimates are shallower and mimic the topography, typically less than 150 m below the surface. Between 2006 and 2010, the depths of rising fluids along the survey profiles remained stable suggesting that hydrothermal activity is in a steady state. This stable activity correlates well with the consistency of the volcanic activity expressed at the surface by the continuously passive degassing.
When compared to previous structural models of the caldera floor, it appears that the diffuse degassing structures have an important effect on the path that shallow groundwater follows to reach the Laguna de Masaya in the eastern part of the caldera. The hydrogeological system is therefore more complex than previously published models and our new structural model implies that the flow of shallow groundwater must bypass the intrusions to reach the Laguna de Masaya. Furthermore, these diffuse degassing structures show clear evidence of activity and must be connected to a shallow magmatic or hydrothermal reservoir beneath the caldera. As such, the heat budget for Masaya must be significantly larger than previously estimated.

Keywords
Masaya, Hydrothermal, Self-potential, Wavelet, Groundwater, Volcano

1. Introduction

Masaya volcano, Nicaragua (11.984°N, 86.161°W, 635 m), is a basaltic shield system consisting of a summit caldera (~11.5 × 6 km) hosting numerous cinder cones, pit craters and fissure vents (McBirney, 1956; Williams, 1983b; Rymer et al., 1998; Acocella, 2007; Harris, 2009) (Fig. 1). The summit caldera is the result of several collapse events (McBirney, 1956; Crenshaw et al., 1982), which are now covered by numerous lava flows that partially fill the caldera (Williams, 1983a; Walker et al., 1993). Since the pioneering work of McBirney (1956), several studies have supported the hypothesis of structural limits controlling the volcanic vent distribution (cinder cones and fissure vents) within the caldera (Williams, 1983a; Maciejewski, 1998), however, different models have been suggested to explain this distribution. Based on field observations, it appears that three of the fissure vents (e.g., the 1772 fissure vent; Fig. 1) have a similar orientation to the main regional Cofradrias fault (N5°E) (Williams, 1983a). Other volcanic structures are oriented differently, such as Masaya cone (N70°E), Nindiri cone (N54°E) and San Pedro fault (N48°E), which suggests a more complex structural influence on the shallow magmatic system (Fig. 1). Field observations suggest that the San Pedro fault (Fig. 2b) is in fact a fissure vent cutting through the west flank of Nindiri cone, starting at the top of San Pedro crater and stopping near Cerro Montozo cone (Fig. 1). On a smaller scale, Masaya and Nindiri cones show signs of collapse with the formation of pit craters (Santiago, San Pedro and San Fernando craters) and subsidence of Nindiri lava lake. Signs of normal faulting are present on the crater walls of Santiago, San Pedro and San Fernando craters (Rymer et al., 1998; Roche et al., 2001; Harris, 2009). Thus, at least in the south part of the caldera, fissure vents and pit craters may be connected at depth by both dykes and faults to a shallow magma chamber. In addition, a normal fault plane (NE–SW strike) associated with fumarolic activity, has been characterized by a previous geophysical study (magnetism and self-potential) across Comalito cone and the fissure vent on the north side of Masaya cone (Pearson, 2010). Earlier geophysical studies (Bouguer gravity mapping), aimed at

* Corresponding author at: Centre for Hydrogeology and Geothermics-CHYN, Université de Neuchâtel, Neuchâtel, Switzerland.
E-mail address: guillaume.mauri@unine.ch (G. Mauri).

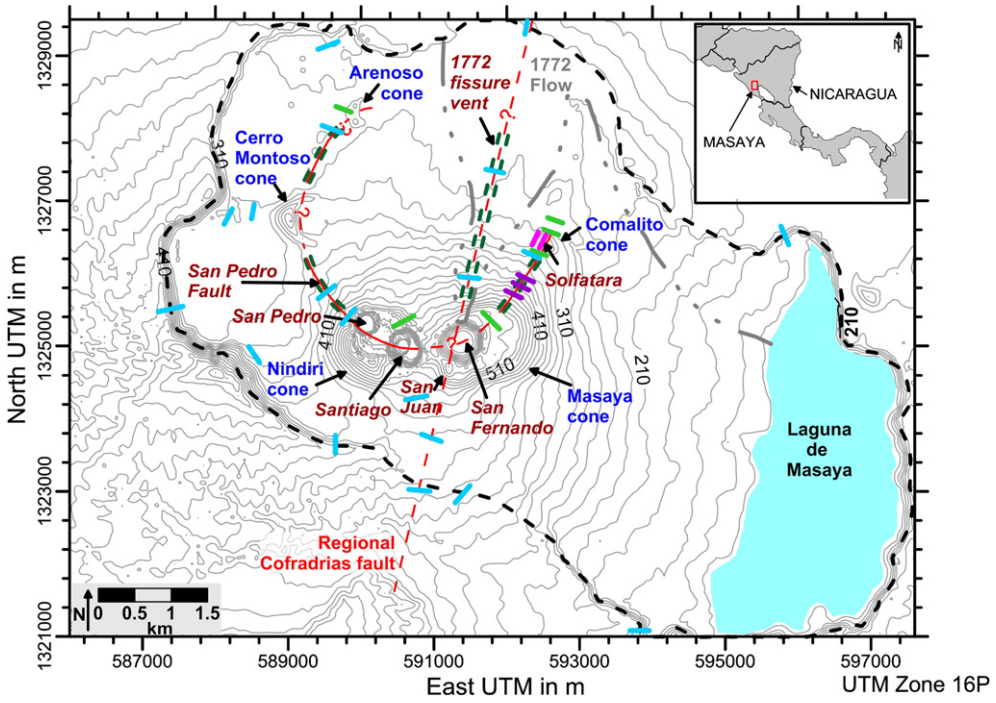

Fig. 1. Masaya caldera, Nicaragua with the post-caldera volcanic cones in blue. The crater names and ground structures are in red. The dark green dashed lines represent the fissure vent structures. Solid red lines are the inferred structure (Crenshaw et al., 1982; Harris, 2009) while the red dashed lines represent hypothetical structures (Crenshaw et al., 1982). The black dashed line is the inferred limit of the caldera. The grey dashed line represents the margins of the 1772 lava flow. Approximate location of previously published soil gas anomalies are represented in light blue (Crenshaw et al., 1982), light green (St-Amand, 1999), pink (Lewicki et al., 2003) and purple (Pearson, 2010). (For interpretation of the references to color in this figure legend, the reader is referred to the web version of this article.)

determining the sources controlling these volcanic structures, were inconclusive due to small density contrasts between the rock formations and insufficient survey stations (Connor and Williams, 1990; Metaxian, 1994). One model suggests that the distribution of both fissure vents and cinder cones is controlled by the regional tensional stress associated to regional faults (Williams, 1983a), while another model suggests that the volcanic structures are associated to cone-sheets or ring-dykes that cut through the caldera (McBirney, 1956; Crenshaw et al., 1982; Maciejewski, 1998). While it is likely that regional faults influence the shallow magmatic system, it is also likely that more local effects, such as depth and shape of a magma chamber, play significant roles in the distribution of the volcanic vents.

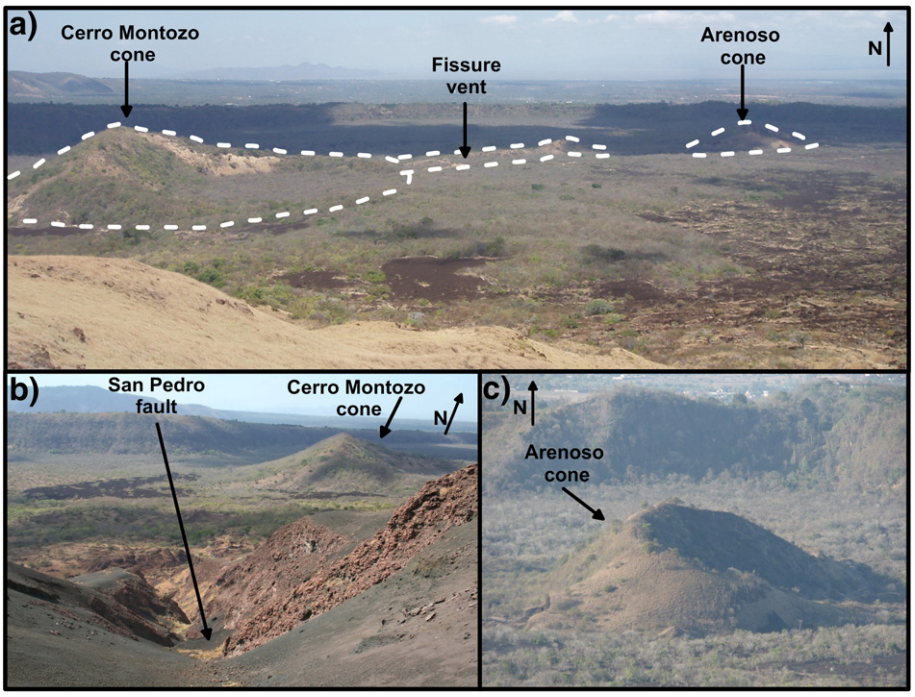

Fig. 2. Field photos showing the lineament of cinder cones and volcanic fissures. a) View of Cerro Montozo cone, Arenoso cone and one volcanic fissure. b) San Pedro fault cutting through Nindiri cone, connects San Pedro crater to Cerro Montoso cone. c) View of Arenoso cone, which is the furthest north of the volcanic cones within Masaya caldera. (For interpretation of the references to color in this figure legend, the reader is referred to the web version of this article.)

Recent significant volcanic activity (small vent-clearing explosions and continuous degassing) originates solely from Santiago crater within the Nindiri cone. The presence and frequent renewal of significant amounts of fresh magma near the surface is physically expressed through continuous degassing (SO_2 flux > 500 t d^{-1}) and variable incandescence in the crater vent (e.g., Stoiber et al., 1986; Williams-Jones et al., 2003; Nadeau and Williams-Jones, 2009). Unlike other persistently active basaltic shield volcanoes which are characterized by frequent effusive eruptions (e.g., Kilauea in Hawaii, Piton de la Fournaise in La Réunion), since the 1800s, Masaya volcano has had only infrequent and volumetrically negligible emissions of juvenile material. The most recent lava flow was erupted in 1772 (McBirney, 1956; Rymer et al., 1998) and covered a significant part of the north sector of the caldera.

Previous studies on gas concentrations and flux (SO_2, CO_2, etc.), gravity, deformation and seismicity have highlighted the existence of an extensive magmatic plumbing system at shallow depths open to the atmosphere through Santiago crater (Crenshaw et al., 1982; Williams, 1983; Walker and Williams, 1986; Stoiber et al., 1986; Walker et al., 1993; Métaxian, 1994; Métaxian et al., 1997; Rymer et al., 1998; Maciejewski, 1998; Roche et al., 2001; Duffell et al., 2003; Williams-Jones et al., 2003), however, the exact depth, volume and shape of this reservoir are still unknown. At Masaya volcano, the continuous presence of fresh magma within a shallow magmatic reservoir is an extraordinarily persistent source of heat and gas (i.e., H_2O, CO_2, SO_2) (Duffell et al., 2003; Martin et al., 2010). In the vicinity of the magma reservoir, the heat will be mainly transferred to the country rock by conduction. While rocks are poor thermal conductors and cannot efficiently transfer heat throughout the entire edifice, volcanic gas and superheated aqueous fluids are excellent thermal conductors, which will both draw the heat from the magma and control heat distribution within the volcanic edifice. Consequently, sustained gas, superheated aqueous fluids and heat flux within the ground could generate and support hydrothermal fluid circulation (Finizola et al., 2002; Chiodini et al., 2005; Bruno et al., 2007; Hase et al., 2010 and references therein). In the case of an open system such as at Masaya volcano, where the magma is directly in contact with the atmosphere, magmatic gases are easily evacuated through the open conduit and thus only a small percentage of the total gas flux may escape diffusely through the surrounding edifice. At Masaya, numerous studies have investigated the low temperature hydrothermal system of Comalito cone (Lewicki et al., 2003; Shaw et al., 2003; Pearson et al., 2008; Pearson, 2010), which has been described as a diffuse degassing structure (DDS) (Chiodini et al., 2005). However, at the caldera scale only a few published studies have looked at the subsurface water flow or distribution of soil gas emissions (Crenshaw et al., 1982; St-Amand, 1999; MacNeil et al., 2007).

Santiago crater, North Masaya fissure vent and Comalito cone are the only active degassing structures known in Masaya caldera, but the volcano has other faults, fracture zones, and cones. Are there other active degassing structures in the caldera? The aim of this study is to investigate the extent of the hydrothermal system throughout the caldera in order to better understand both groundwater flow and the shallow volcanic structures and their effect on the current and future volcanic activity. Five geophysical surveys were thus performed between February 2006 and March 2010 to collect ~81 km of self-potential electrical profiles, ~ 7.5 km of soil CO_2 concentration and ~6.5 km of ground temperature measurements (Fig. 3). Profiles of these measurements were then used to study the spatial and temporal variations of groundwater flow while multiscale wavelet tomography applied to the self-potential data enabled characterization of water depths (Mauri et al., 2010, 2011).

2. Groundwater flow in active calderas

On active volcanoes, hydrogeological structures are always complex and groundwater flow may be vertically stratified in several layers, which may be connected through vertical water flow along faults and geological discontinuities (e.g., Zlotnicki et al., 1998; Finizola et al., 2002; Pribnow et al., 2003; Bruno et al., 2007). Very often within the hydrogeological structure, one or several hydrothermal systems may be present and supported by the volcanic heat/gas flow rising through the edifice (Finizola et al., 2002; Pribnow et al., 2003). When not associated with active crater vents, these hydrothermal systems can represent diffuse degassing structures (DDS) in which ground permeability is higher due to faults or fractures (Chiodini et al., 2001, 2005). The DDS can act as preferential channels between the deep aquifer and the surface while in other parts of the volcanic edifice, the groundwater may consist solely of cold water flow. There are numerous examples of these hydrogeological systems such as on Usu and Aso volcanoes (Japan), Long Valley caldera and the Hawaiian Islands (USA) (Peterson, 1972; Sorey et al., 1991; Hase et al., 2005; Hase et al., 2010). As calderas are usually characterized by a topographic depression, it is common to find groundwater flow within the volcanic rocks as well as sizeable bodies of water on their surface (e.g., Farrar et al., 2003; Pribnow et al., 2003; Join et al., 2005; Pagli et al., 2006; Zlotnicki et al., 2009; Todesco et al., 2010).

Hydrodynamic and chemical features of groundwater depend on the physical and chemical properties of the host rock (i.e., porosity, permeability, chemical composition, temperature, Seaber, 1988; Al-Aswad and Al-Bassam, 1997), however, without well information, it is often difficult to determine these properties. For this study, no well data are available, thus it is not possible to describe groundwater flow through its physical parameters (porosity, permeability). However, the groundwater flow direction can be characterized through the self-potential elevation gradient (see Section 4.1) (Lénat, 2007). Therefore, as in other studies (e.g., Zlotnicki et al., 1998; Lénat, 2007; Finizola et al., 2009 and references therein) and independent of its chemical composition, groundwater flow will be separated into two groups based on the flow direction:

The first group, called gravitational flow (GF), includes any groundwater flow having its flow direction characterized mainly by a horizontal component. The second group, the uprising flow (UF) comprises any groundwater flow characterized by a major vertical component of the flow direction. When the fluid pressure becomes stronger than gravitational forces, groundwater rises along the structural limit (e.g., fault plane, rock discontinuities) having the highest hydraulic conductivity. The uprising flow is also called artesian flow when it reaches the surface (Banton and Bangoy, 1997) and is always the consequence of increased fluid pressure. This can be due to two processes. First, when the uprising flow originates from a confined or semi-confined aquifer, the fluid pressure builds up within the confined zone due to limited space (Banton and Bangoy, 1997; Drever, 1997). Second, when the uprising flow originates from a geothermal reservoir hot enough that the fluid may exist in two phases (liquid and gas), gas dilatation will increase fluid pressure within the reservoir causing the fluid to rise toward the surface (Johnston et al., 2001; Zlotnicki and Nishida, 2003; Legaz et al., 2009).

In order to distinguish rising hydrothermal fluid (unconfined or confined) from cold fluids (unconfined or confined), it is important to determine the three key characteristics that represent an uprising hydrothermal flow, notably flow direction, soil gas concentration and anomalous ground temperature (Finizola et al., 2002, 2009 and references therein).

3. Methods

3.1. Self-potential

Self-potential (SP) is a passive electrical method which measures the natural electrical current present in the ground and is commonly used to investigate groundwater flow direction (Corwin and Hoover, 1979; Ishido and Mizutani, 1981; Zlotnicki et al., 1994, 1998; Finizola

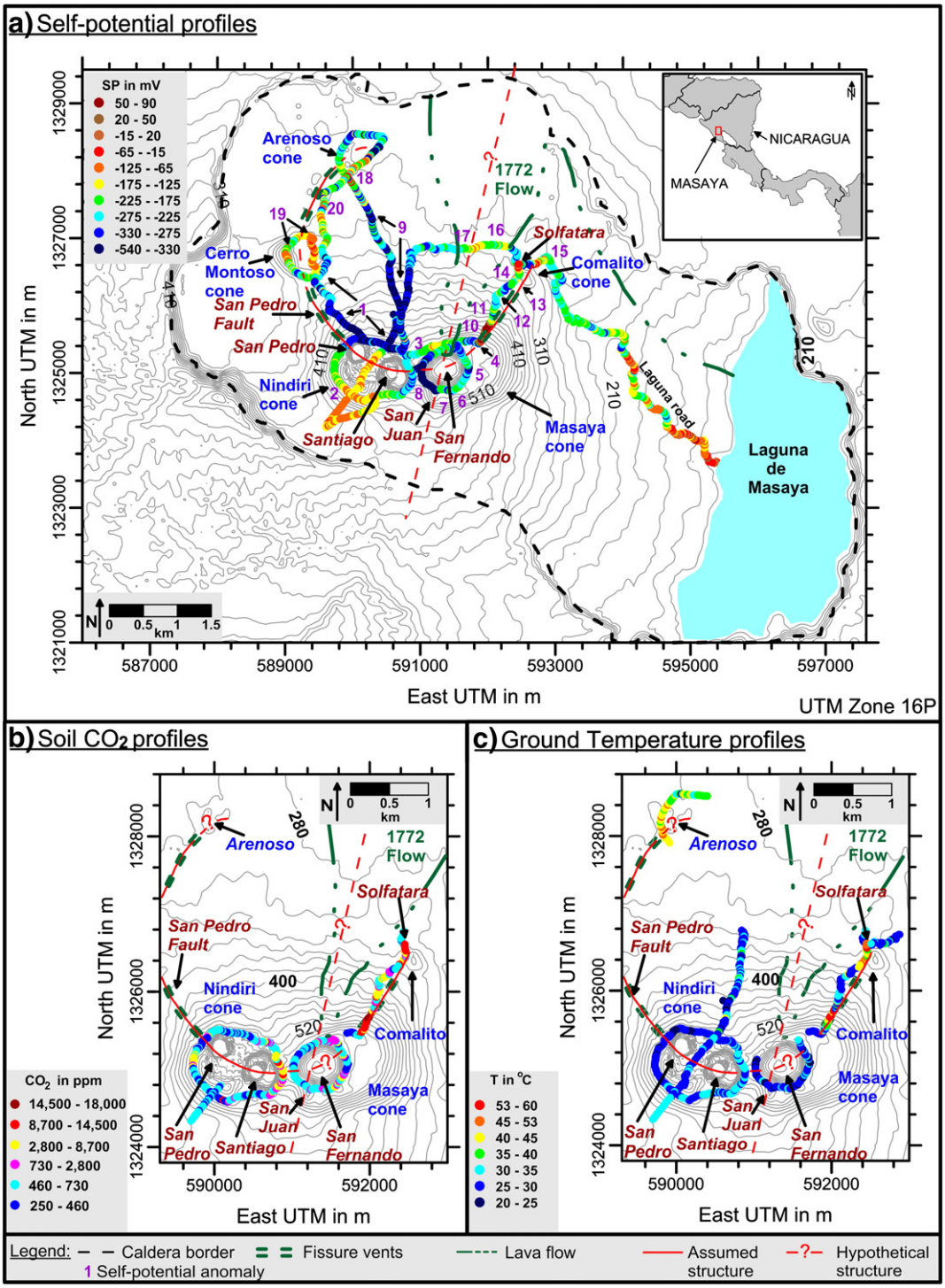

Fig. 3. Map of the profile measurements made between 2006 and 2010 in Masaya caldera, Nicaragua. a) Self-potential profiles overlain on the tectonic setting presented in Fig. 1. b) Soil CO_2 gas profiles measured in 2008 on Masaya caldera. c) Ground temperature measurements collected between 2007 and 2010. Note the different scales. See text for description of the representation method. (For interpretation of the references to color in this figure legend, the reader is referred to the web version of this article.)

et al., 2002; Zlotnicki and Nishida, 2003; Lénat, 2007; Jouniaux et al., 2009 and references therein). A natural electrical current is generated by a number of different processes which include several physical and chemical phenomena. The most important sources of electrical generation are the electrokinetic, rapid fluid disruption and thermoelectric processes.

The electrokinetic process (EK) is a complex phenomenon, which occurs when water flows through a porous medium (e.g., Corwin and Hoover, 1979; Jouniaux and Pozzy, 1995; Hase et al., 2003; Aizawa et al., 2008; Jouniaux et al., 2009). EK is affected by several key parameters including the chemical composition of the water and the zeta potential, which is the electrical expression of the interaction between ions along the Helmholtz double layer (Hase et al., 2003; Aizawa et al., 2008). With an increase in flow pressure, the quantity of ions removed from the surface of minerals constituting the rock will increase. The result is the generation of electrical potential due to differential displacement between the ions present in solution and ions on the Helmholtz double layers which form the polarized

mineral (Avena and DePauli, 1996; Guichet and Zuddas, 2003; Hase et al., 2003). Rapid fluid disruption (RFD) is an ephemeral phenomenon which characterizes water phase changes from liquid to vapor and will be expressed by an increase of the rising water flux (Johnston et al., 2001). The thermoelectric process occurs when heat flux (e.g., due to magmatic intrusions) is applied to a rock generating a thermal gradient by conduction (Corwin and Hoover, 1979). All of these processes are always related in some way to a differential displacement of ions in the ground.

For both the electrokinetic process and RFD, the ions are moved via fluid flow (liquid or gas), while for the thermoelectric process, the ions move through heat transfer by conduction in the rock. Another significant phenomenon is the effect of heterogeneous ground resistivity on the electrical potential (Sailhac and Marquis, 2001; Saracco et al., 2004). Previous studies (e.g., Minsley et al., 2007) have shown that resistivity contrasts, when not spatially associated with water flow (i.e., electrokinetic effect), may in some instances be of significant importance. In this study, however, and based on previous work, the main resistivity contrasts are considered to be associated with the pathway of the main ground water flow (MacNeil et al., 2007; Mauri et al., 2010). A more detailed description of self-potential electrical generation can be found in the literature (Ewing, 1939; Poldini, 1939; Corwin and Hoover, 1979; Avena and DePauli, 1996; Johnston et al., 2001; Guichet and Zuddas, 2003; Hase et al., 2003; Zlotnicki and Nishida, 2003; Lénat, 2007; Aizawa et al., 2008; Finizola et al., 2009; Jouniaux et al., 2009).

On Masaya volcano, RFD is considered to be the main electrical source generation process in the hydrothermal environment, such as in the Comalito solfatara (Lewicki et al., 2003; Pearson et al., 2008). Otherwise, the electrokinetic process is the main source of electrical generation due to gravitational ground water flow (Lewicki et al., 2003). Thus, both the electrokinetic effect and RFD are considered as the source of electrical generation on Masaya volcano.

In this study, self-potential surveys were made using two copper electrodes, consisting of a copper rod in a saturated copper-sulphate solution, connected to a 350 m long insulated copper wire cable and a high impedance (100 MOhm) multimeter. A sampling step of 20 m was used and the profiles were organized in interconnected loops to control the SP drift, which was never more than 40 mV. Electrode polarization was controlled at least twice a day and never exceeded more than 2 mV and generally was close to 0 mV. A total of ~81 km of profiles were completed between 2006 and 2010 (Fig. 3a).

3.2. Soil CO_2 concentration

The first magmatic gas to exsolve from the magma, CO_2, rises preferentially through magma and country rock along the main structural faults (e.g., Finizola et al., 2004; Chiodini et al., 2005; Bruno et al., 2007). While atmospheric CO_2 concentrations range from ~350 to 500 ppm, magmatic gas can generate CO_2 concentrations from <1% to >95% within the soil pore spaces (e.g., Williams-Jones et al., 2000; Federico et al., 2010). However, biogenic activity may also release CO_2 through the root systems and generate up to a few 1000 ppm CO_2 (e.g., Widén and Majdi, 2001). There are likely multiple sources for the diffuse CO_2 and accurate discrimination of these sources requires carbon isotope analyses (e.g., Chiodini et al., 2008) that were beyond the scope of this study. Therefore, for this study, CO_2 ground concentrations between 400 and 1000 ppm are only considered to be potentially of magmatic origin if the surrounding vegetation is null or sparse. Measurements of soil CO_2 gas concentrations were made by inserting a probe 60 cm into the ground and pumping the gas to a sensor. The CO_2-meter (a GM70 with GMP221 probe by Vaisala Inc.) can accurately record concentrations up to 20%, with an error of 0.02% CO_2 + 2% of the reading value. Soil CO_2 concentration measurements were made with a sampling step of 20 m in the same location as the self-potential measurements. In order to detect and control any drift of the device calibration, atmospheric CO_2 concentration was measured at least each 100 m, but generally every 20 m. Soil CO_2 concentration profiles were measured in 2008 and cover a distance of 7.5 km (Fig. 3b).

3.3. Ground temperature

Hot/boiling gas and hydrothermal fluids lose their heat by conduction to the surrounding ground and by condensation of the gas. Over a short period of time (1 day or less), the ground temperature at more than 30 cm depth, is relatively well protected from diurnal temperature variation due to the poor thermal conduction of soil. Over longer time periods (weeks, months), atmospheric temperature variation can affect ground temperature to 1 m below the surface (Pearson et al., 2008). On Masaya volcano, diurnal temperature variations are less than 5 °C in amplitude, rain events can generate variations of 5 °C and volcanic events can cause a temperature variation up to 10 °C over a short period of time (less than 1 day) (Pearson et al., 2008). When no magmatic heat source is present, the temperature of the ground is commonly below the atmospheric temperature (> 20 °C). When the ground is heated by hot rising gas or hot/boiling hydrothermal fluids, the ground temperature can reach 75 °C on Masaya volcano (Lewicki et al., 2003; Pearson et al., 2008; Pearson, 2010). On other volcanoes, ground temperature can reach more than 300 °C and is usually linked with CO_2 gas anomalies and thus allows for detection of the main fracture pathways (e.g., Finizola et al., 2004; Chiodini et al., 2005; Bruno et al., 2007 and references there in).

Ground temperature measurements were made with a temperature probe (K-type chrome-aluminum probe) having an accuracy of ~0.2 °C. Measurements were carried out at a depth greater than 30 cm with a sampling step of 20 m in the same location as both the self-potential and soil CO_2 measurements. In order to avoid artifacts due to the influence of the atmosphere, atmospheric temperature was measured at least once every 100 m (Fig. 3c); as no volcanic events (e.g., vent explosion), nor rainfall occurred during the measurements, the diurnal variation is considered to be less than 5 °C. Thus any ground temperature anomaly higher than 10 °C above atmospheric temperature can be considered to be due to hydrothermal activity only.

4. Analysis

4.1. SP/elevation gradient

The self-potential method generally allows for the differentiation of gravitational groundwater flow (GF) from uprising hydrothermal fluids (UF) by evaluation of the SP/elevation gradient (e.g., Finizola et al., 2004; Lénat, 2007; Finizola et al., 2009). However, it is not always unambiguous and more information from soil CO_2 concentration and ground temperature is required to differentiate sources of SP anomalies. For greatest accuracy, the SP/elevation gradient must be calculated on an SP profile made along the main slope direction, which is assumed to match that of the water flow. When an SP profile crosses a slope perpendicular to the main slope, it is not always possible to accurately characterize the type of groundwater flow. In this case, if no other SP profiles or other data (e.g., CO_2 concentration, ground temperature) are available, the SP anomaly is uncertain and may be attributed to gravitational groundwater flow until further information becomes available.

In this study, a hydrothermal system is considered to be the source of an SP anomaly when the SP/elevation gradient is symmetrically positive along a sub-horizontal surface to its associated SP anomaly, or when the SP/elevation gradient is asymmetric along a slope (Lénat, 2007). When all three anomalies (SP, soil gas concentration

and ground temperature) are present, it can be interpreted with confidence that a hydrothermal system is present (Zlotnicki et al., 1998; Finizola et al., 2002, 2009). However, it is not always possible to acquire data from all three methods, thus when the SP/elevation gradient clearly shows a hydrothermal signature such as described in the literature (e.g., Lénat, 2007), this study considers it to be relevant.

4.2. Multi-scale wavelet tomography

Multi-scale wavelet tomography (MWT) is a signal processing method based on continuous wavelet transform (CWT) (e.g., Grossmann and Morlet, 1984; Saracco, 1994). When multi-scale wavelet tomography is used with the Poisson kernel family and applied to potential field data, it allows for depth determination of the object generating the measured potential field anomaly (Moreau et al., 1997, 1999; Fedi and Quarta, 1998; Sailhac et al., 2000; Gibert and Pessel, 2001; Sailhac and Marquis, 2001; Saracco et al., 2004; Fedi et al., 2005; Cooper, 2006; Fedi, 2007; Saracco et al., 2007; Mauri et al., 2010). MWT on self-potential data allows us to estimate the depth of the electrical source, which in the case of groundwater flow is the main flow pathway (Sailhac and Marquis, 2001; Saracco et al., 2004, Mauri et al., 2010). As shown by previous studies, the effect of a strongly heterogeneous resistivity medium (contrast of 3 orders of magnitude) on CWT depth accuracy can be efficiently mitigated by making multiple analyses (Mauri et al., 2010). Based on the Poisson kernel family, this study uses the following four real wavelets: second ($n=2$) and third ($n=3$) vertical derivative (V2 and V3, respectively) and second and third horizontal derivative (H2 and H3, respectively). These wavelets allow for location of dipole (in 1D, $\alpha=$ -2 and in 2D, $\alpha=$ -3) and monopole (in 1D, $\alpha=-1$ and in 2D, $\alpha=-2$) sources, which correspond to the electrical anomalies generated by water flow through bedrock (Sailhac and Marquis, 2001; Zlotnicki and Nishida, 2003; Saracco et al., 2004; Lénat, 2007). In order to obtain reliable source depths, each 1D self-potential profile was analyzed using the MWTmat code (Mauri et al., 2011) with 500 dilations on a range of dilation from 1 to 15 for each of the four analyzing wavelets. Only depths found with at least three of the four wavelet analyses are considered significant. A more detailed description of MWT can be found in the works of Saracco et al. (2007) and Mauri et al. (2010, 2011) and references therein.

5. Results and discussion

In order to spatially represent, without interpolation errors, the self-potential, soil CO_2 concentration and ground temperature data across the caldera, each data point was presented by a colored dot (Fig. 3); the color scales were chosen to best represent the structure shown in the profiles (Figs. 4 to 8). Water flow directions and type are based on the profile analyses summarized in Table 1.

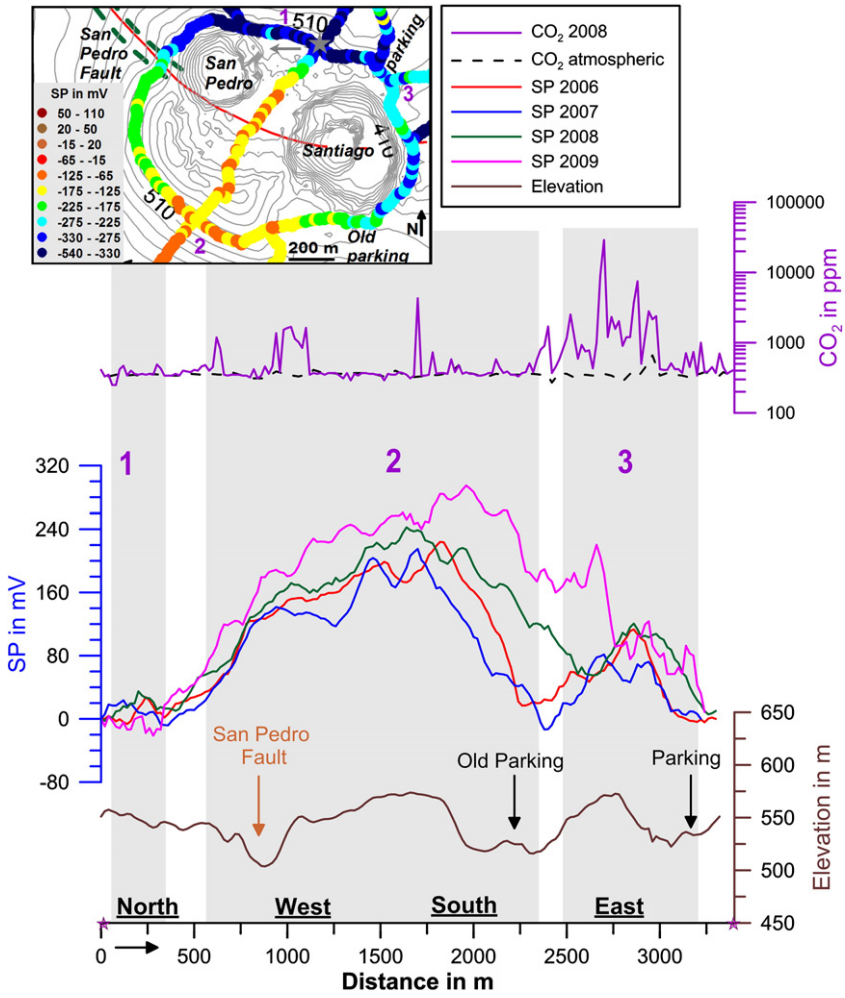

Fig. 4. Self-potential (5 point moving average), CO_2 concentration and topography of the survey profile around Nindiri crater measured between 2006 and 2009. All self-potential profiles are referenced to the same base station on the north rim of Nindiri, which is assumed to be stable over time and to which a 0 mV value has been attributed to facilitate the comparison between different surveys. The purple numbers (and shaded areas) represent the anomalies reported in Table 1. Sampling step is 20 m. The stars indicate the beginning and end of the profile. (For interpretation of the references to color in this figure legend, the reader is referred to the web version of this article.)

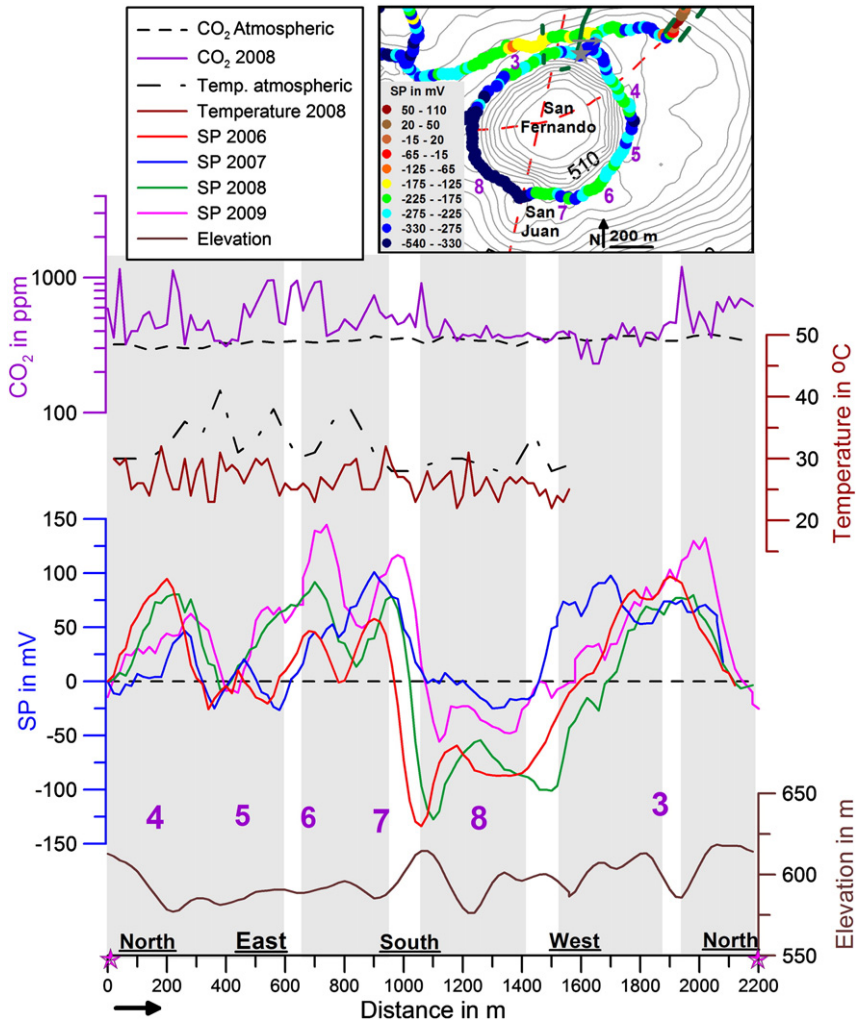

Fig. 5. Self-potential, CO_2 soil concentration, ground temperature and topography of the survey profile around Masaya crater measured between 2006 and 2009. All self-potential profiles are referenced to the same base station on the north rim of the crater of Masaya, which is assumed to be stable over time and to which a 0 mV value has been attributed to facilitate comparison between different surveys. The purple numbers (and shaded areas) represent the anomalies reported in Table 1. Sampling step is 20 m. The star indicates the beginning and end of the profile. (For interpretation of the references to color in this figure legend, the reader is referred to the web version of this article.)

5.1. Self-potential data

In order to best organize the different electrical anomalies present on the different self-potential profiles, the self-potential/elevation gradient was chosen as the discriminant parameter to characterize each structure. Each electrical anomaly is numbered and grouped by geographical position. Although the presented self-potential profiles have been smoothed (5 point moving average, Figs. 4 to 8), the analyses of each profile by SP-elevation gradient were made with unsmoothed profiles.

Based on their strong negative self-potential/elevation gradient (and often associated with strong negative SP values), several electrical anomalies are interpreted as gravitational downward water flow (Table 1, anomaly #1, #8, #9, #16) and represented in Fig. 3a by the blue colors (dark and light patterns). These gravitational flows are found on the south-east part of San Fernando crater on Masaya cone and throughout the caldera floor zone located within an area encircled by the main volcanic cones (Fig. 3a). This study finds no evidence for distinct individual gravitational flow systems, which is consistent with the MacNeil et al. (2007) hydrogeological model and supports the existence of a single gravitational groundwater system that flows throughout the caldera floor towards the Laguna de Masaya. As such, gravitational flows (Table 1, anomaly #1, #8, #9, #16) are considered to represent different areas of the same groundwater system.

On the eastern part of Masaya caldera, along the Laguna road from Comalito cone to Laguna de Masaya, several electrical anomalies are present (Fig. 3a), however, this self-potential profile is the only section that is not closed in a loop and thus cannot be corrected for SP drift. As such, these anomalies cannot be properly defined by the self-potential/elevation gradient. However, as they were found both in 2007 and 2008, these electrical anomalies are likely not due to noise and could be actual anomalies showing local irregularities in the water table, subsurface resistivity or in hydrothermal circulation.

In the western part of Masaya caldera, as all SP profiles are in a loop and thus properly corrected for any SP drift, it was possible to characterize fifteen electrical anomalies. These SP anomalies show both positive and negative SP/elevation gradients (Table 1, anomalies # 2 to #6, #10 to #15, #17 to #19), which indicate uprising water flow at depth. Furthermore, these anomalies are present on each of the cinder cones (Nindiri cone in Fig. 4, Masaya cone in Fig. 5, Comalito cone in Fig. 6, Cerro Montozo in Fig. 8 and Arenoso in Fig. 3a), but also within the caldera floor (e.g., fissure vent near Arenoso, Fig. 3a; beneath the 1772 lava flow on

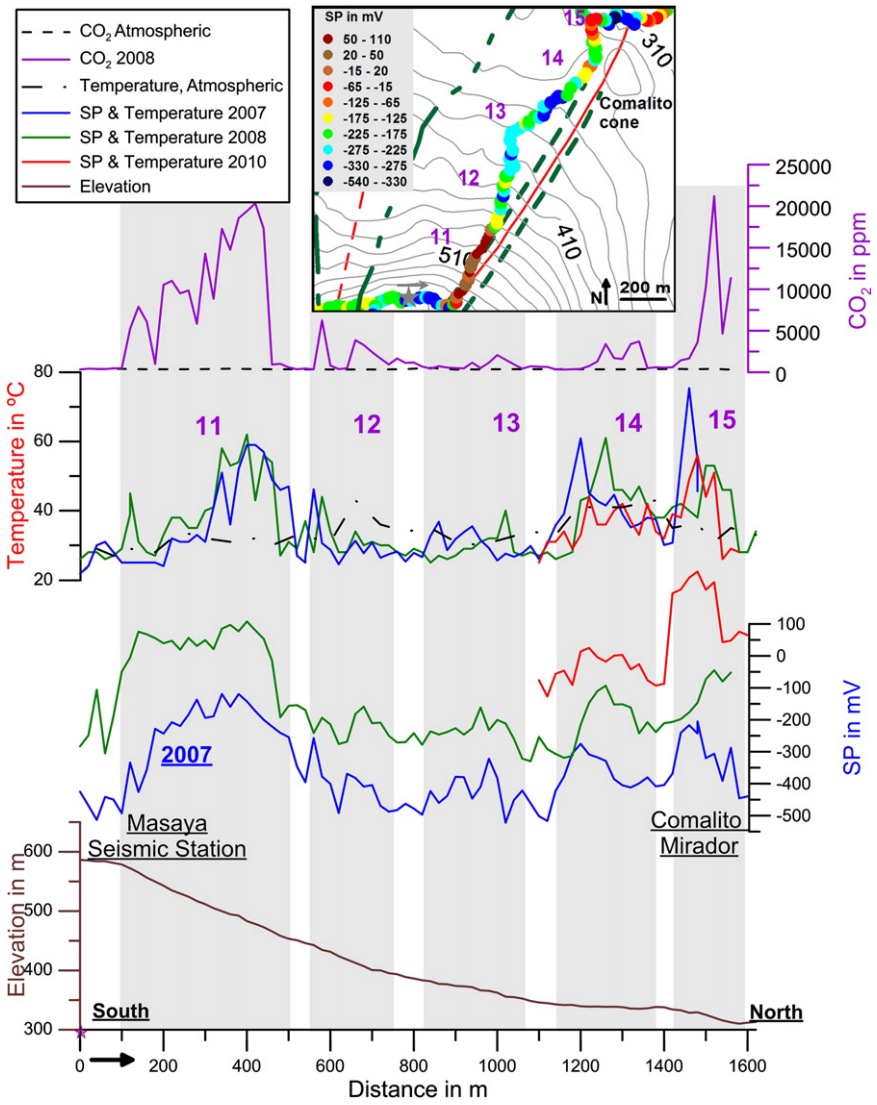

Fig. 6. Self-potential, CO_2 concentration, temperature and topography of the survey profile across the north flank of Masaya cone to the solfatara of Comalito measured in 2007 and 2008. All self-potential profiles are referenced to the same base station at the Laguna de Masaya, which is assumed to be stable over time and to which a 0 mV value has been attributed to facilitate comparison of the different surveys. The purple numbers (and shaded areas) represent the anomalies reported in Table 1. Sampling step is 20 m. The star indicates the beginning and end of the profile. (For interpretation of the references to color in this figure legend, the reader is referred to the web version of this article.)

Fig. 7). Based on the self-potential mapping, the different uprising flows do not, at least on the surface, appear to be spatially connected to each other; each is thus named after its geographic position (Table 1).

5.2. Ground temperature

Ground temperature anomalies have only been found in the Comalito solfatara (mean of 43 ºC ± 8 ºC with a peak of 74 ºC in 2007) and on the fissure vent cutting through the north slope of Masaya cone (Fig. 6). From year to year, the ground temperatures in these two areas show similar amplitudes. Ground temperature anomalies correlate each time with self-potential anomalies and asymmetric self-potential/elevation gradients, which represent uprising fluids (Fig. 6, Table 1). These ground temperature anomalies also correlate with measured soil CO_2 concentrations (Fig. 6, Table 1). Our results support the previous observations for this area and show a similar extent to other studies (Lewicki et al., 2003; Pearson, 2010). In the other mapped areas, only the west and north side of Arenoso cone show anomalous ground temperatures (40 ºC ± 5 ºC, #18, Table 1). Otherwise the measured ground temperature variations are always correlated with measured atmospheric variations.

5.3. Soil gas concentrations

Previous isotopic studies of the CO_2 gas measured on Comalito cone have shown that the CO_2 was the result of a mixture of mantle and deep carbonate sources (Lewicki et al., 2003) and that passive CO_2 degassing in the caldera was associated to diffuse degassing structures (DDS) (Chiodini et al., 2005). Other studies have shown anomalous soil CO_2 concentrations on Arenoso cone and on the upper north rim of Masaya cone (St-Amand, 1999; Pearson, 2010). In the early 1980s, a radon and mercury gas study also suggested the presence of faults on the caldera floor (Fig. 1), which correspond to the Cofradrias fault as well as to a hypothetical buried circular structure along the main volcanic features (e.g., Nindiri cone, Masaya cone, Comalito, Arenoso and the western fissure vents) (Crenshaw et al., 1982).

The measured soil CO_2 concentration anomalies from this study show a good correlation with the location of previously suggested faults (Fig. 3). Even though the spatial extent of the survey represents

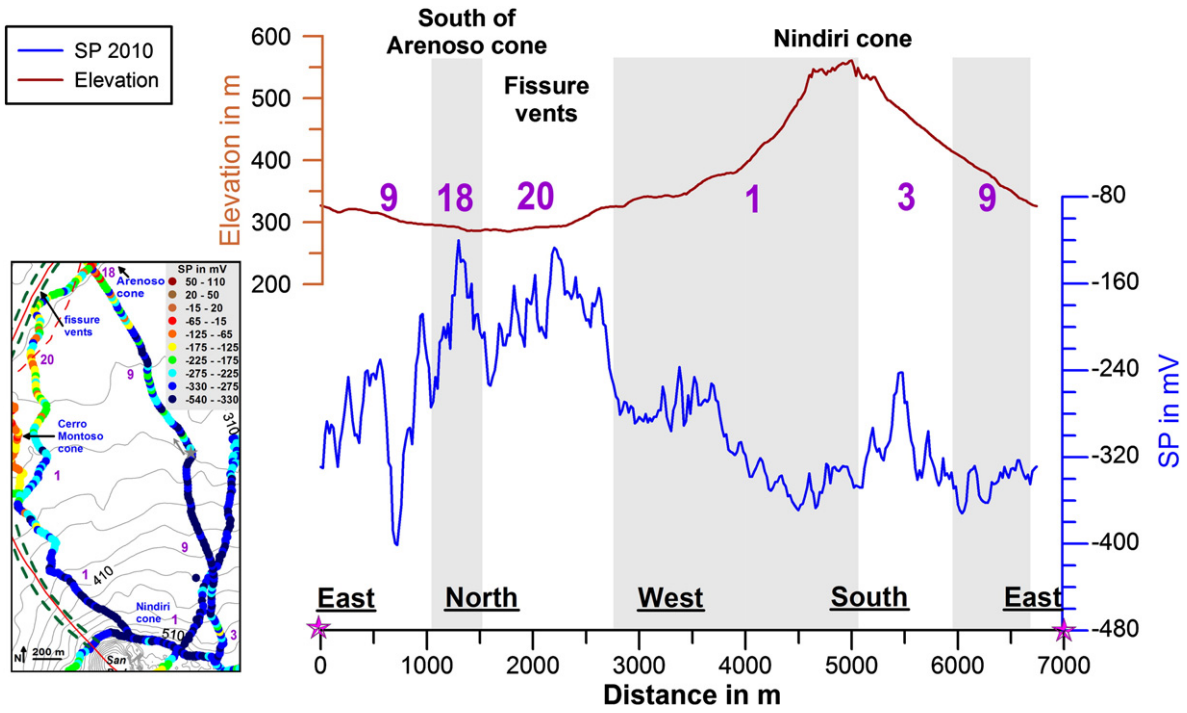

Fig. 7. Self-potential survey on the north part of Masaya caldera. All the self-potential profiles are referenced at the same base station to the Laguna de Masaya, which is assumed to be stable over time and to which a 0 mV value has been attributed to facilitate comparison between different surveys. Sampling step is 20 m. The purple numbers (and shaded areas) represent the anomalies (Table 1). The star indicates the beginning of the profile. (For interpretation of the references to color in this figure legend, the reader is referred to the web version of this article.)

only 7.5 km of profile, it is clear that the stronger degassing area found by this study is located in the fissure vent cutting through the north slope of Masaya. This large anomaly (400 m in length) has a mean concentration of 9,363 ppm with a maximum of ~20,000 ppm and has good spatial co-variations with both ground temperature and self-potential anomalies (#11, Fig. 6). Another area showing significant amounts of soil CO_2 is the solfatara of Comalito (Table 1, #15, Fig. 3), also detected in other studies (Lewicki et al., 2003; Chiodini et al., 2005; Pearson, 2010). As shown in the work of Crenshaw et al. (1982), a north–south fault cuts through San Fernando crater on Masaya cone and appears to coincide with both a diffuse CO_2 and SP anomaly measured in this study (#3, Fig. 5).

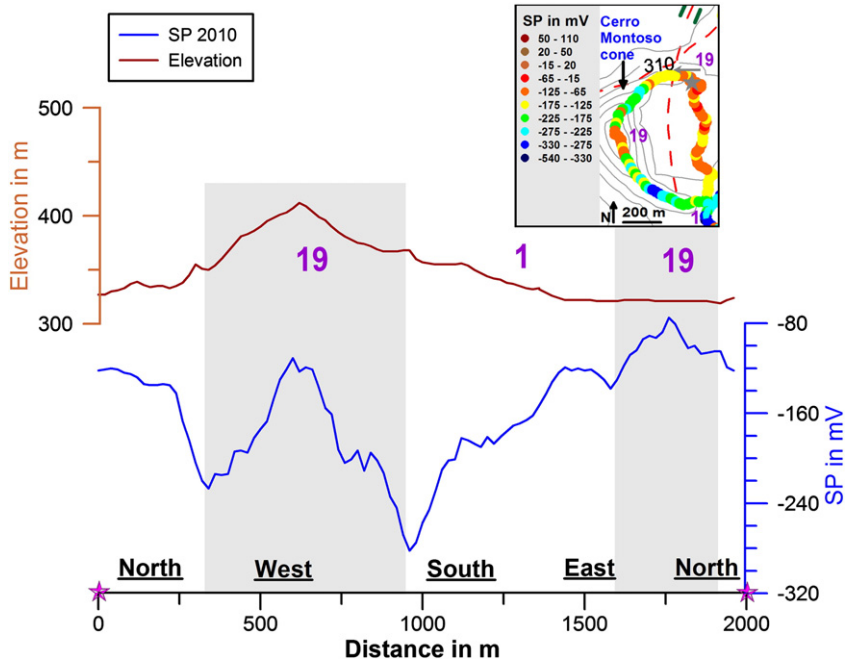

Fig. 8. Self-potential profile of the survey across Cerro Montoso cone measured in 2010. All the self-potential profiles have been corrected for drift and level has been shifted to match the 2008 reference level which is the base station at the Laguna de Masaya. The purple numbers The purple numbers (and shaded areas) represent the anomalies reported in Table 1. Sampling step is 20 m. The star indicates the beginning and end of the profile. (For interpretation of the references to color in this figure legend, the reader is referred to the web version of this article.)

Table 1
Description of the different anomalies based on the self-potential amplitude, SP/elevation gradient, ground temperature and soil gas measurements between 2008 and 2010. North, South, East, West and Center are the local direction in comparison to the center of each of the anomalies. *Nan*: no data exist for the associated SP anomaly. *Und*: SP vs. elevation data is undefined because it shows no significant trend and could not be translated into an SP/elevation gradient. *GF*: gravitational flow. *H.S.*: hydrothermal system. [a] from the work of Crenshaw et al. (1982); [b] from the work of Lewicki et al. (2003); [c] from the work of St-Amand (1999); [d] from the work of Pearson (2010). Rank represents the certainty on the determination of the anomaly and is organized in three levels of certainty. Rank A, the anomaly is characterized by all SP, soil gas and ground temperature data. Rank B, the anomaly is characterized by SP and ground temperature data. Rank C, the anomaly is characterized by both gas data from the literature and SP data. Rank D, the anomaly is characterized by SP data only.

SP anomaly	Flow structure name	Profile length (m)	SP ampl. (mV)	SP/elevation gradient (mV m^{-1})					Ground temp. (ºC)		CO_2 soil gas conc. (ppm)		Previous soil gas studies (presence)			Rank
				N	S	E	W	C	Mean	σ	Mean	σ	Rn	Hg	CO_2	
1	GF	1000	200	−0.3	Nan	−1.6	−0.7	Nan	26	2	368	54	No	No	Nan	A
2	Nindiri HS	1500	200	−3.7	−0.2	+1.4	Und	Nan	28	2	521	509	Yes[a]	Yes[a]	Nan	A
3	Masaya-Nindiri Junction HS	500	150	−4.3	−1.3	+4.5	−0.5	Nan	30	2	1934	4318	Nan	Nan	Nan	A
4	NE Masaya HS	300	100	−2.3	Nan	+11.4	Nan	Nan	27	3	549	260	Yes[a]	Yes[a]	Nan	A
5, 6	SE Masaya HS	500	100	Nan	−7.3	+6	Nan	Nan	27	2	584	233	Nan	Nan	Nan	A
7	San Juan HS	260	180	Nan	Nan	+1.4	−9.9	Nan	28	3	532	115	Nan	Nan	Nan	A
8	GF	300	80	Nan	−1.5	Nan	−1.9	Nan	26	2	427	131	Nan	Nan	Nan	A
9	GF	1500	150	−3	−1	−12.6	−58.8	Nan	29	3	Nan	Nan	Nan	Nan	Nan	B
10, 11	Masaya N. slope HS	600	300	+11.5	−9.3	Nan	Nan	-0.4	41	11	9363	6601	Nan	Nan	Yes[c]	A
12	Masaya N. slope HS	200	150	+2.2	+4.9	Nan	Nan	Nan	32	5	2233	1952	Nan	Nan	Yes[d]	A
13	Comalito HS	150	100	+4.9	−2.7	Nan	Nan	Nan	29	4	801	458	Yes[a]	Yes[a]	Yes[b,c,d]	A
14, 15	Comalito HS	200	200	−7.2	−56.9	+38	+20.7	-10.5	43	8	4202	5354	Yes[a]	Yes[a]	Yes[b,c,d]	A
16	GF	300	120	Nan	Nan	−17.3	−46.7	Nan	Nan	Nan	Nan	Nan	No	No	Nan	D
17	1772 lava flow HS	650	100	+20	−4.6	Nan	Nan	Nan	Nan	Nan	Nan	Nan	No	No	Nan	D
18	Arenoso HS	500	100	+3.5	+20.3	Und	Nan	Nan	40	5	Nan	Nan	Yes[a]	Yes[a]	Yes[c]	B
19	Cerro Montoso HS	700	300	Und	+2.6	Nan	+2.2	Nan	Nan	Nan	Nan	Nan	Nan	Nan	Nan	D
20	Vent fissure HS	1300	160	6.54	−0.69	Nan	Nan	Nan	Nan	Nan	Nan	Nan	Yes[a]	Yes[a]	Nan	C

5.4. Groundwater depth

Multi-scale wavelet tomography of the 5 years of SP profiles resulted in more than 500 depth values that represent the depths of the main electrical generation sources, interpreted as main groundwater pathways. The MWT analyses have been done on smoothed profiles (5 point moving average) to remove high frequency noise. To avoid artifact depths, only estimated depths found with at least 3 of the 4 analyzing wavelets are considered significant (Appendix 1). By comparing the horizontal position of each anomaly associated to each depth, it was possible to characterize 31 time-series data sets, which represent 99 individual depths well localized in space (GPS, depth) and time (from 2006 to 2010) (Table 2, Appendix 1).

While the spatial distribution of the water depths are limited to the self-potential coverage of the caldera, the estimated water depths relative to the topographic surface are quite constant across the caldera following the topographic variation (Table 2). 47% of the water depths are between 50 and 100 m below the topographic surface and 83% of the depths are less than 150 m below the topographic surface. A similar distribution is found if the depths are discriminated between uprising water and gravitational water flow (Table 2). In addition, each depth value has an error bar (one standard deviation, σz) which represents the scattering of all the raw estimated depths associated to this value; σz is less than 50 m for 79% of the estimated depths and the mean of the error for the 99 estimated depths is 36 m (min. value of 11 m and max. of 68 m, Table 3). Similar values were found on a north-south profile across Nindiri (Mauri et al., 2010) and have been included in this study (diamonds and squares on Fig. 9b,d). Further north, within both Cerro Montoso and Arenoso cones, the water depth is between 50 to 120 m below the surface (Table 1, Appendix 1). Even within the fissure on the north slope of Masaya and on the Comalito solfatara, where the uprising flows are associated with the strongest hydrothermal activity, the water depth is between 30 to 120 m below the surface (Fig. 11). Finally, away from the volcanic structures on the caldera floor, where the water flow is associated with gravitational flow, the water depths show similar patterns between 30 and 110 m below the surface (Fig. 12).

The MWT on self-potential data can only detect the shallowest water structure, any other structure below it will have its electrical signal overprinted by the shallowest one and as such, the deeper structures cannot be characterized. A model by MacNeil et al. (2007) proposed a groundwater structure consisting of a series of overlying groundwater flow; the deeper layer is strongly affected by water vaporization near the active vent of Santiago crater while the shallowest groundwater layer mimics the topography flowing from the cones towards the Laguna de Masaya. The water depth calculation

Table 2
Scattering of the depth values (σz) and significance of water depth interpretation. The scattering of the individual data can be found in Appendix 1.

	All system types		Gravitational flow		Uprising flow	
	Depth	%	Depth	%	Depth	%
Total	99	100	33	100	66	100
Shallower than 50 m	13	13	7	21	6	9
Between 50 and 100 m	47	47	14	42	33	50
Between 100 and 150 m	23	23	6	18	17	26
Between 150 and 200 m	14	14	5	15	9	14
Deeper than 200 m	2	2	1	3	1	2

Table 3
Number of depths for both aquifer and hydrothermal systems based on the results of Appendix 1. Statistics of the estimated depths are from the multi-scale wavelet tomography on self-potential data.

Scattering of the vertical depth values (σz in m) between 2006 and 2010						
s	11	σz max	68	σz mean	36	
Range of	All depths		Uprising flow		Gravitational flow	
σz	Nbr	%	Nbr	%	Nbr	%
All σz	99	100	66	100	33	100
less than <10	0	0	0	0	0	0
σz<20	14	14	8	12	6	18
σz<30	36	36	21	32	15	45
σz<40	63	64	42	64	21	64
σz<50	78	79	53	80	25	76
σz<60	90	91	61	92	29	88
σz<70	99	100	66	100	33	100

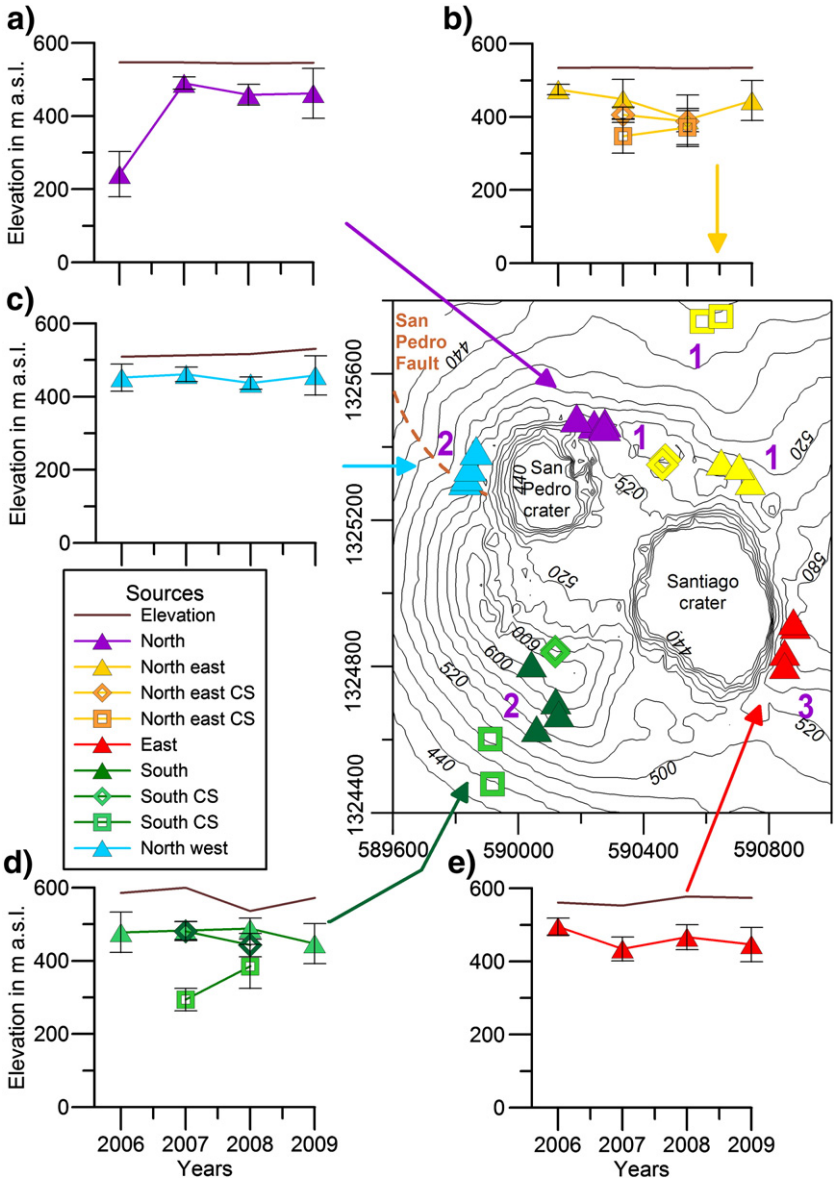

Fig. 9. Water depths between 2006 and 2009 on Nindiri cone. Horizontal GPS coordinates and depths of the water are obtained by multi-scale wavelet tomography applied on the self-potential survey loop. Triangles represent depths calculated from the MWT analysis of the Nindiri survey loop (Fig. 5). Squares and diamonds are calculated depths from the MWT analysis of a Nindiri cross-section SP profile (from Mauri et al., 2010). All depths are presented in Appendix 1. (For interpretation of the references to color in this figure legend, the reader is referred to the web version of this article.)

by MWT on SP data clearly shows the shallow water layer, although the depth is ~100 m shallower than previously modeled by MacNeil et al. (2007).

This discrepancy in depth is likely due to differences in the sensitivity of each method. While the TEM method will characterize the large resistivity contrast associated to transition between the more conductive saturated zone and the less conductive unsaturated zone, the MWT method characterizes the main groundwater flow responsible for electrical generation. On one hand, TEM may not be sufficiently sensitive to detect a thin saturated zone in a complex heterogeneous volcanic subsurface with variable resistivity layers. On the other hand, self-potential records the electrical field generated by fluid flow inside the shallowest saturated zone, allowing MWT on SP data to detect it independent of the thickness of the saturated zone. It is also possible that the presence of a high resistivity contrast (not associated to an aquifer) could disrupt the electrical signal recorded by the SP. However, this does not seem likely as the TEM data show a normal decrease of apparent ground resistivity with increasing depth (MacNeil et al., 2007). Lacking any direct well data, it is difficult to determine which model best represents the true water depth.

Another possibility regarding the relatively shallow estimated depths is that there is locally significant water flowing within the unsaturated zone. However, such water circulation in the unsaturated zone is unlikely because field measurements were made during the dry season. Regarding the depth of the uprising flow associated to the DDS, due to their limited surface extent, it is possible that they were not detected by the transient electromagnetic method (TEM) used in the work of MacNeil et al. (2007). Previous numerical models (Pearson, 2010) of the Comalito and North Masaya fissure support the idea of a water table at ~250 m below the surface from which a localized escape path along fault allows the hot fluids to rise to the topographic surface. From a self-potential generation perspective, the hot uprising fluids, which generate a RFD electrical anomaly, would overprint the EK electrical generation from the underlying aquifer. Thus, the MWT water depths for the DDS correspond to the escape path along faults rather than the underlying aquifer.

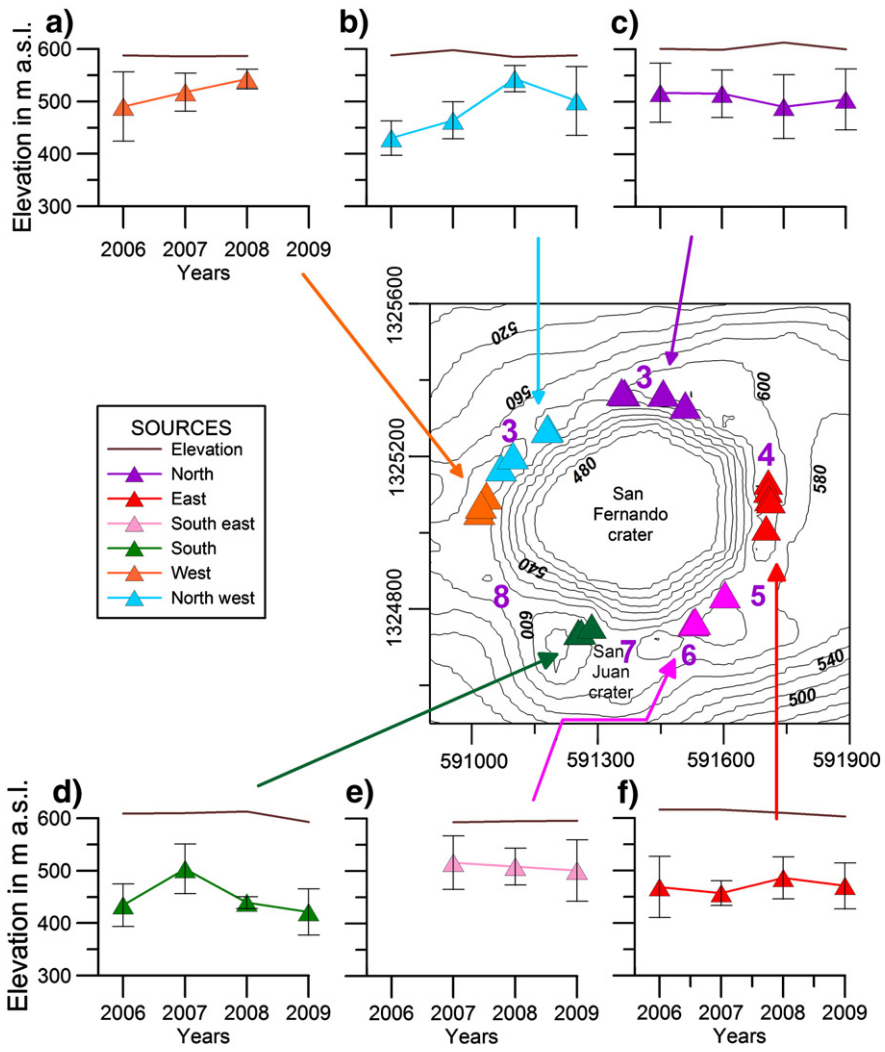

Fig. 10. Water depths between 2006 and 2009 around Masaya crater. Horizontal GPS coordinates and depths of the water are obtained by multi-scale wavelet tomography applied to the self-potential survey loop. Triangles represent depths calculated from the MWT of the Masaya SP survey loop (Fig. 5). All depths are presented in Appendix 1. (For interpretation of the references to color in this figure legend, the reader is referred to the web version of this article.)

Over the period from 2006 to 2010, there was no significant change in the persistent volcanic activity of Masaya volcano (Martin et al., 2010). Over the same period of time, this study has shown that within both Masaya and Nindiri cones, the depth of the groundwater flow did not vary within the uncertainty of the depth value (σz) (Figs. 9, 10). In addition, similar depth stability is found in both the Comalito cone solfatara and Masaya north fissure (Fig. 11). Consequently, while the uncertainty on the depth value (σz) makes it difficult to characterize any significant depth variation over time, the relative depth stability of groundwater flow may be due to the persistence of Masaya volcanic activity.

5.5. Diffuse degassing structures

As previously reported (e.g., McBirney, 1956; Crenshaw et al., 1982; Williams, 1983b), a number of structures related to previous collapse events and faults crosscut the caldera (solid lines and dashed red lines on Fig. 13a). Fault displacements, if any, have been covered by recent lava flows making it impossible to characterize them over time and the only expression left of the inner structural limits are cinder cones and fissure vents (Fig. 13a).

The Comalito hydrothermal system has been described as a diffuse degassing structure (DDS) (Chiodini et al., 2005) due to the spatially well-defined area affected by passive degassing and anomalous ground temperature. The self-potential results presented here and in previous studies (Lewicki et al., 2003; Pearson, 2010) show that the Comalito DDS is also characterized by uprising groundwater flow (Table 1, anomalies #13, 14, 15). On active volcanoes, uprising groundwater flow is typically associated with uprising hydrothermal flow based on the self-potential-elevation gradient (Lénat, 2007). In the case of Masaya volcano, we may thus extend the definition of DDS to be any area where both passive degassing and uprising groundwater flows are present and associated with ground temperature anomalies. On each of the five cinder cones within the caldera, uprising flows have been detected from SP-elevation gradients and each is associated with soil gas anomalies (Table 1, anomalies # 2 to #6, #10 to #15, #17 to #19) suggesting that Arenoso, Nindiri, Masaya cones and the north Masaya fissure vent are also diffuse degassing structures. While no soil CO_2 concentration or ground temperature data are available for Cerro Montoso cone, uprising flow was detected by the positive SP-elevation gradient (Table 1, #19) suggesting that Cerro Montoso cone is also a diffuse degassing structure.

Although the fissure vent between Arenoso and Cerro Montoso cone is only partially covered by the SP survey, it appears to be associated with a positive SP anomaly (Table 1, Fig. 7, #20) as well as with radon and mercury gas anomalies (Fig. 1; Crenshaw et al. (1982)). Similarly, the San Pedro fault, crossed only by the SP survey at its junction with Nindiri cone, is associated with a strong increase in SP

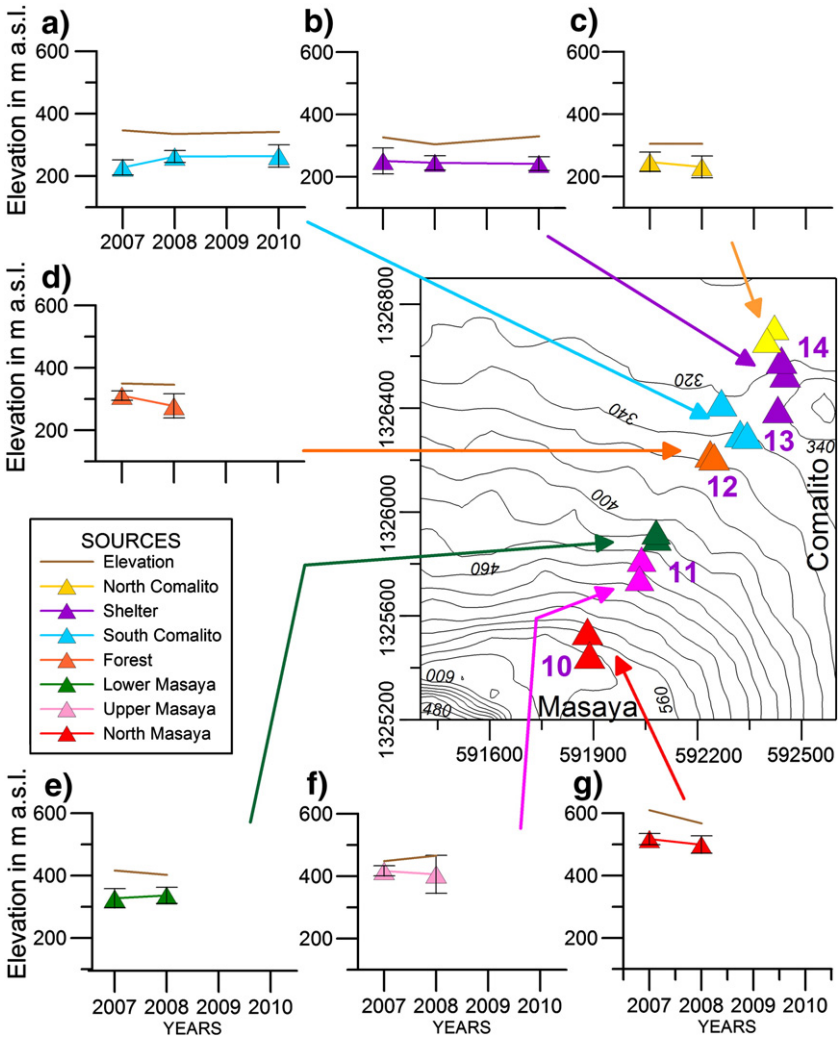

Fig. 11. Water depths between 2007 and 2010 across the north flank of Masaya cone until the solfatara of Comalito cone. Horizontal GPS coordinates and depths of the water are obtained by multi-scale wavelet tomography applied on the self-potential survey loop. Triangles represent depths calculated from the MWT of the Comalito profile (Fig. 6). All depths are presented in Appendix 1. (For interpretation of the references to color in this figure legend, the reader is referred to the web version of this article.)

amplitude, low diffuse CO_2 concentration and radon and mercury gas anomalies (Fig. 4; Crenshaw et al. (1982)). These two fissure vents should therefore also be considered as diffuse degassing structures.

At the caldera scale, the DDS structures are spatially organized in a semi-circular shape that define inner structural limits (Fig. 13a). On the surface, these inner structural limits consist of volcanic cones and fissure vents, while at depth, they likely consist of dykes and faults cutting through the caldera floor, which act as preferential pathways for the hot rising hydrothermal fluids of the DDS structures. Importantly, this evidence for widespread hydrothermal activity raises significant questions regarding quantification of the thermal budget of the caldera complex and highlights the need for a more extensive caldera-wide degassing study (e.g., Chiodini et al., 2001).

5.6. Hydrogeological systems

With an understanding of the active caldera structures and groundwater depths, it then becomes possible to develop a groundwater flow model for Masaya (Fig. 13b, c). Near the active vent of Santiago crater, groundwater is likely vaporized at depth leading to depletion of the deep water reservoir detected by MacNeil et al. (2007) (grey dashed line on Fig. 13b) and must thus be recharged via infiltration along caldera rim structures or other structural limits not detected by this study. During the rainy season, an unknown quantity of precipitation will infiltrate the caldera floor to recharge the shallowest aquifer and possibly the deep aquifer. Away from the caldera rim and associated with the diffuse degassing structures, the inner structural limits likely consist of intruded dykes and faults cutting through the caldera floor; these are expressed on the surface by volcanic cones and fissure vents (Fig. 13a). Results from self-potential, soil gas concentrations and ground temperatures suggest that each hydrothermal zone present in the caldera is associated to these inner structural limits, which allow fluids to move from the deepest aquifer to the shallowest aquifer. The presence of hot rising fluids (gas, water) indicates that these inner structural limits are moving heat and gas from depth (red stars on Fig. 13b, c), the source of which is likely the shallow magmatic system, but which cannot be characterized from our results. These hydrothermal fluids will rise due to increased fluid pressure through the more fractured part of the caldera.

In contrast, the shallow gravitational water flow generally mimics the topography of the caldera from the west to north and then eastward, until Laguna de Masaya. The top of the shallowest groundwater layer, based on the MWT analyses, is generally at less than 150 m below the topographic surface. In terms of elevation, the hydrothermal fluids and aquifer range from 141 m to 542 m a.s.l. (Appendix 1), which locate the groundwater above the lake surface (119 m a.s.l.). This result supports the previous model where the general flow direction is toward

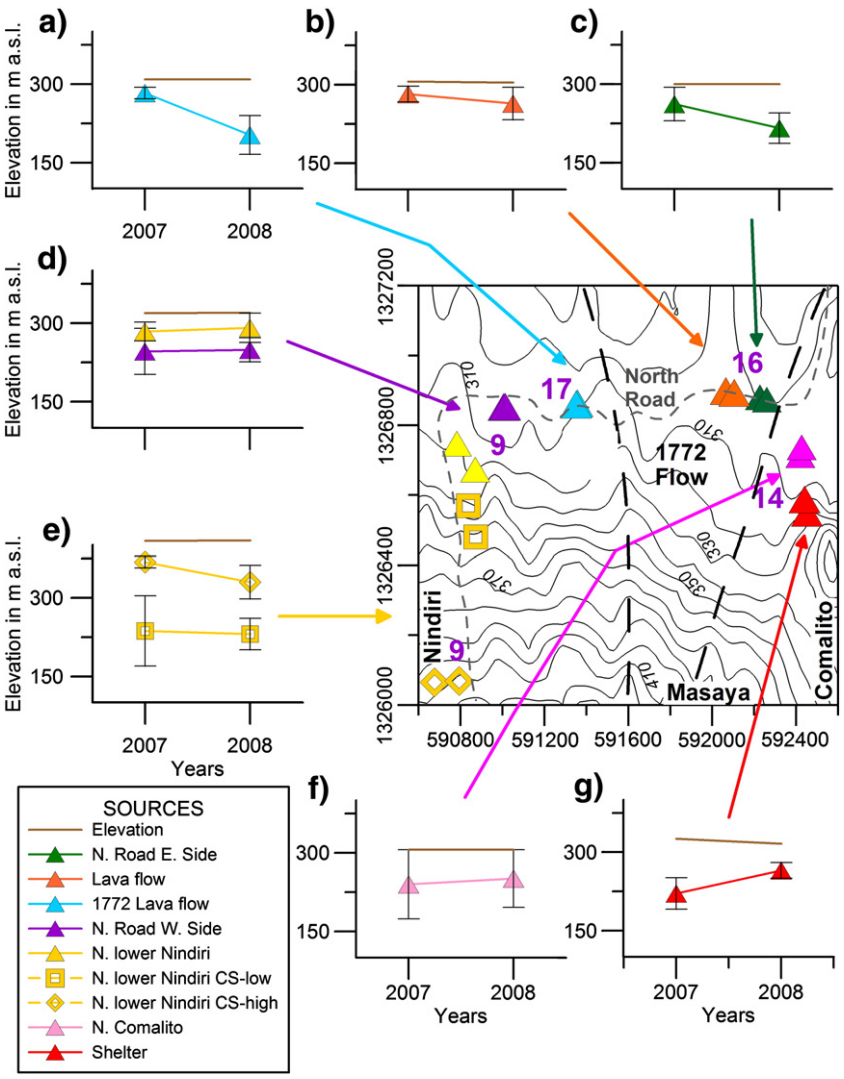

Fig. 12. Water depths between 2007 and 2008 along North road. Horizontal GPS coordinates and depths of the water are obtained by multi-scale wavelet tomography applied on the self-potential survey loop. Triangles represent depths calculated from the MWT of the North road (Fig. 3a). Squares and diamonds are depths calculated from the MWT analysis of the Nindiri cross-section SP profile (Mauri et al., 2010). All depths are presented in Appendix 1. (For interpretation of the references to color in this figure legend, the reader is referred to the web version of this article.)

the lake whose surface represents the level of the deep aquifer (Fig. 13b, c) (MacNeil et al., 2007). However, our updated model highlights the significant role of the inner structural limits, which act as barriers in the north part of the caldera and force the water flow around them (Fig. 13a). As the roots of the inner structural limits, dykes likely connect the cones and fissure vents at the surface to the shallow magmatic reservoir at depth. Such sub-vertical to vertical dense intrusions will act as hydraulic barriers forcing the flow northward. This is clearly the case on the north side of the summit cones, where the shallow aquifer mimics the topographic decrease toward the northern caldera rim; near the north caldera rim, the flow direction then turns eastward to the lake.

6. Conclusion

This study presents an updated groundwater flow model that incorporates and highlights the existence of active volcanic structures cutting across the caldera floor. Multi-scale wavelet tomography on 5 years of self-potential surveys across Masaya volcano show that the shallowest groundwater flow mimics the topography, usually less than 150 m below the surface. Furthermore, uprising fluids are present within each of the five cinder cones and three volcanic fissures across the caldera; self-potential, ground temperature and soil CO_2 surveys show that these fluids are hydrothermal in origin.

Fig. 13. Groundwater flow model for Masaya volcano. a) Spatial localization of uprising fluids associated to hydrothermal activity (green diamonds) and gravitational water flow (blue squares) within Masaya caldera for which depths have been determined (see Appendix 1 and text for description). The names of volcanic cones are in blue. The crater names and ground structures are in dark red. The dark green dashed lines are the fissure vent structures. Solid red lines represent the inferred structures (faults, fissures) (Crenshaw et al., 1982; Harris, 2009). The red dashed lines are the hypothetical structures (faults, fissures) (Crenshaw et al., 1982). The black dashed line is the inferred limit of the caldera. Depth values can be found in Appendix 1. See text for description. b) Cross-section along profile A-D-B representing the water flow direction across the caldera. c) Cross-section along profile C-D-B representing the water flow direction through the active Santiago crater and across the caldera. The dashed red lines represent underground structures where the dip orientation is unknown and are based on the work of Williams (1983a,b) and Crenshaw et al. (1982). Solid arrows represent the flow direction inferred from the self-potential/elevation gradient. Elevations of the shallow flow direction estimated from MWT are in blue and solid green arrows. The dashed grey line and dashed blue arrows are hypothetical deep flow from TEM results (MacNeil et al., 2007). Dot above a blue line represents water flow having a flow direction different than the cross-section view. (For interpretation of the references to color in this figure legend, the reader is referred to the web version of this article.)

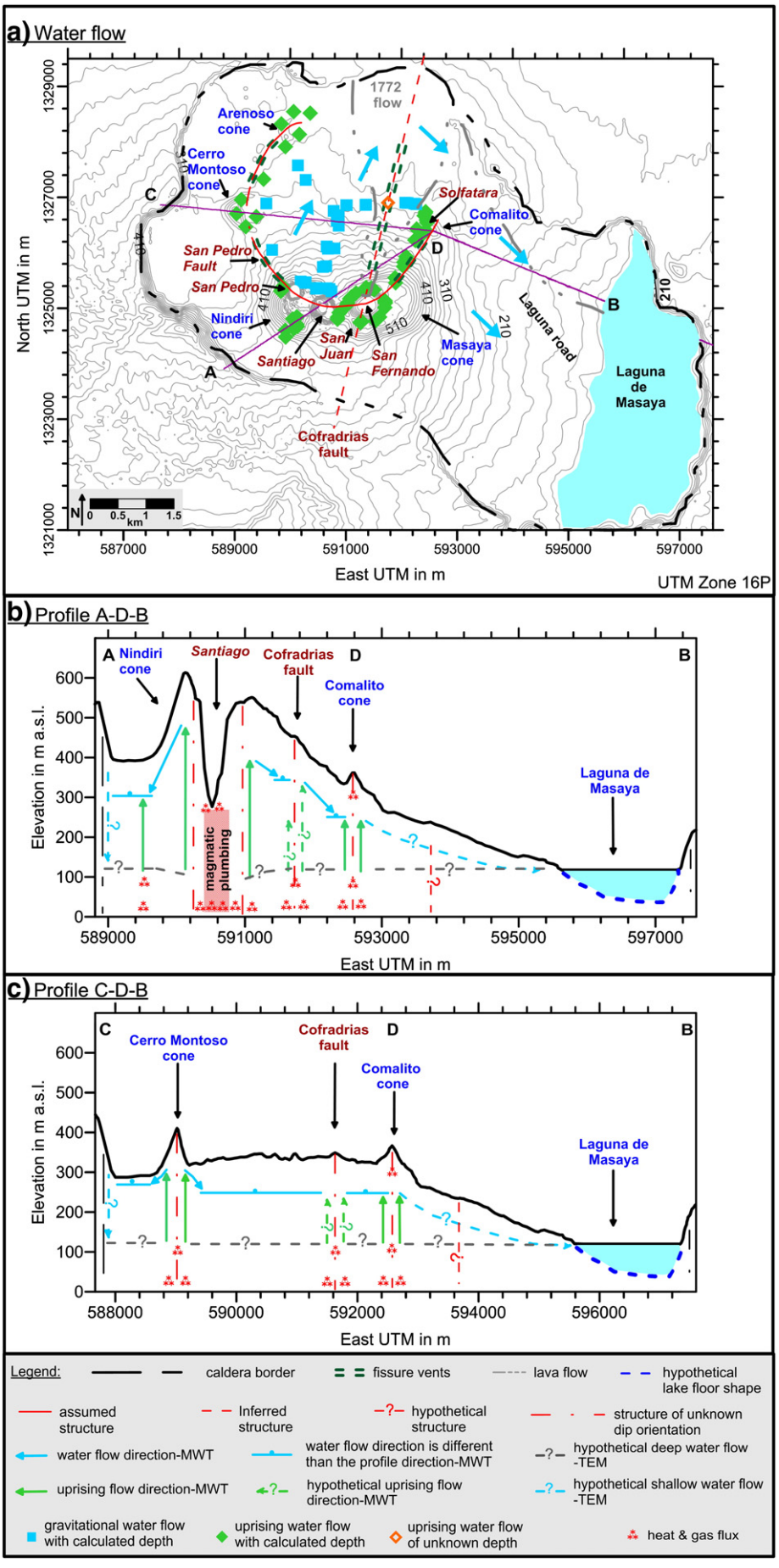
a) Water flow
1772 flow
Arenoso cone
Cerro Montoso cone
Solfatara
Comalito cone
San Pedro Fault
San Pedro
Nindiri cone
Santiago
San Juan
San Fernando
Masaya cone
Laguna road
Laguna de Masaya
Cofradrias fault
A
B
C
D
410
310
210
510
North UTM in m
East UTM in m
UTM Zone 16P
b) Profile A-D-B
Nindiri cone
Santiago
Cofradrias fault
Comalito cone
magmatic plumbing
Laguna de Masaya
Elevation in m a.s.l.
East UTM in m
c) Profile C-D-B
Cerro Montoso cone
Cofradrias fault
Comalito cone
Laguna de Masaya
Elevation in m a.s.l.
East UTM in m
Legend:
caldera border
fissure vents
lava flow
hypothetical lake floor shape
assumed structure
Inferred structure
hypothetical structure
structure of unknown dip orientation
water flow direction-MWT
water flow direction is different than the profile direction-MWT
hypothetical deep water flow -TEM
uprising flow direction-MWT
hypothetical uprising flow direction-MWT
hypothetical shallow water flow -TEM
gravitational water flow with calculated depth
uprising water flow with calculated depth
uprising water flow of unknown depth
heat & gas flux

The presence of faults, fissures and dikes have two different effects on the hydrogeological system of Masaya volcano. The inner semi-circular structure will channel the uprising hydrothermal fluid, while also acting as a barrier to lateral gravitational water flow. Furthermore, the uprising water and hot magmatic gas escaping along these interconnected structures indicate that these structures are active pathways to both hydrothermal systems and the shallow magmatic reservoir. The shallow hydrothermal system is widespread throughout the caldera and as such, the heat budget for the central part of Masaya must be significantly larger than previously thought.

Diffuse degassing structures are clearly not limited to the Comalito solfatara but are found throughout the caldera and as such, any significant change within the magmatic reservoir may affect the hot fluids rising along the DDS. For example, the injection of new magma at depth would likely increase both gas and heat flux in the DDS fluids leading to stronger SP anomalies on the surface. Such changes in SP have been detected on other volcanoes preceding eruptions (e.g., Finizola et al., 2009) and depth changes in the rising fluids can be detected by MWT on SP data (e.g., Saracco et al., 2004). While Masaya volcano was in a steady state from 2006 to 2010 with no significant change in fluid depth detected, multi-scale wavelet tomography of self-potential surveys has proved to be an effective method for delineating active subsurface structures and monitoring fluctuations in hydrothermal systems that may precede changes in volcanic activity.

Supplementary materials related to this article can be found online at doi:10.1016/j.jvolgeores.2012.02.003.

Acknowledgments

This research was supported by an NSERC Discovery grant to G. Williams-Jones. The authors thank one anonymous reviewer, J-F. Lénat, O. Merle, G. Bertrand for their constructive comments. Many thanks to the Dirección General de Geofísica of INETER and the Parque Nacional Volcán Masaya for their continued support in Nicaragua. This study would not have been possible without the help of a large number of volunteer student field assistants.

References

Acocella, V., 2007. Understanding caldera structure and development: an overview of analogue models compared to natural calderas. Earth-Science Reviews 85 (3–4), 125–160. doi:10.1016/j.earscirev.2007.08.004.

Aizawa, K., Uyeshima, M., Nogami, K., 2008. Zeta potential estimation of volcanic rocks on 11 island arc-type volcanoes in Japan: implication for the generation of local self-potential anomalies. Journal of Geophysical Research 113, B02201. doi:10.1029/2007JB005058.

Al-Aswad, A.A., Al-Bassam, A.M., 1997. Proposed hydrostratigraphical classification and nomenclature application to the Palaeozoic in Saudi Arabia. Journal of African Earth Sciences 24 (4), 497–510. doi:10.1016/S0899-5362(97)00077-8.

Avena, M.J., DePauli, C.P., 1996. Modeling the interfacial properties of an amorphous aluminosilicate dispersed in aqueous NaCl solutions. Colloids and Surfaces A Physicochemical and Engineering Aspects 118 (1–2), 75–87.

Banton, O., Bangoy, L.M., 1997. Hydrogeologie, multiscience ennvironnmentale des eaux souterraines (Hydrologeology, environmental multiscience of groundwater). Presses de l'Universite du Quebec/AUPELF, Sainte-Foy, Quebec. 460 pp.

Bruno, P.P.G., Ricciardi, G.P., Petrillo, Z., Di Fiore, V., Troiano, A., Chiodini, G., 2007. Geophysical and hydrogeological experiments from a shallow hydrothermal system at Solfatara Volcano, Campi Flegrei, Italy: response to caldera unrest. Journal of Geophysical Research 112, B6201. doi:10.1029/2006JB004383.

Chiodini, G., Frondini, F., Cardellini, C., Granieri, D., Marini, L., Ventura, G., 2001. CO2 degassing and energy release at Solfatara Volcano, Campi Flegrei, Italy. Journal of Geophysical Research 106 (B8), 16,213–16,221.

Chiodini, G., Granieri, D., Avino, R., Caliro, S., Costa, A., Werner, C., 2005. Carbon dioxide diffuse degassing and estimation of heat release from volcanic and hydrothermal systems. Journal of Geophysical Research 110, B8204. doi:10.1029/2004JB003542.

Chiodini, G., Caliro, S., Cardellini, C., Avino, R., Granieri, D., Schmidt, A., 2008. Carbon isotopic composition of soil CO_2 efflux, a powerful method to discriminate different sources feeding soil CO_2 degassing in volcanic-hydrothermal areas. Earth and Planetary Science Letters 274, 372–379. doi:10.1016/j.epsl.2008.07.051.

Connor, C.B., Williams, S.N., 1990. Interpretation of gravity anomalies, Masaya caldera complex, Nicaragua. In: Larue, D.K., Draper, G. (Eds.), Transactions 12th Caribbean Geological Conference, St. Croix, U.S. Virgin Islands Aug. 1989, pp. 495–502.

Cooper, G.R.J., 2006. Interpreting potential field data using continuous wavelet transforms of their horizontal derivatives. Computers & Geosciences 32 (7), 984–992.

Corwin, R.F., Hoover, D.B., 1979. Self-potential method in geothermal exploration. Geophysics 44 (2), 226–245.

Crenshaw, W.B., Williams, S.N., Stoiber, R.E., 1982. Fault location by radon and mercury detection at an active volcano in Nicaragua. Nature 300, 345–346.

Drever, J.I., 1997. The geochemistry of natural waters, surface and groundwater environments, Third edition. Prentice Hall. 436 pp.

Duffell, H.J., Oppenheimer, C., Pyle, D.M., Galle, B., McGonigle, A.J.S., Burton, M.R., 2003. Changes in gas composition prior to a minor explosive eruption at Masaya volcano, Nicaragua. Journal of Volcanology and Geothermal Research 126 (2), 327–339. doi:10.1016/S0377-0273(03)00156-2.

Ewing, S., 1939. The copper–copper sulfate half-cell for measuring potentials in earth. American Gas Association, Proceedings 21, 624–634.

Farrar, C.D., Sorey, M.L., Roelo¡s, E., Galloway, D.L., Howle, J.F., Jacobson, R., 2003. Inferences on the hydrothermal system beneath the resurgent dome in Long Valley caldera, from recent flow testing and geochemical sampling. Journal of Volcanology and Geothermal Research 127, 305–328.

Federico, C., Corso, P.P., Fiordilino, E., Cardellini, C., Chiodini, G., Parello, F., Pisciotta, A., 2010. CO_2 degassing at La Solfatara volcano (Phlegrean Fields): processes affecting $\delta^{13}C$ and $\delta^{18}O$ of soil CO_2. Geochimica et Cosmochimica Acta 74 (12), 3521–3538. doi:10.1016/j.gca.2010.03.010.

Fedi, M., 2007. DEXP: a fast method to determine the depth and the structural index of potential fields sources. Geophysics 72, I1–I11.

Fedi, M., Quarta, T., 1998. Wavelet analysis for the regional-residual and local separation of potential field anomalies. Geophysical Prospecting 46 (5), 507–525.

Fedi, M., Paoletti, V., Rapolla, A., 2005. The role of multilevel data in potential field interpretation. Computers & Geosciences 31 (6), 681–688.

Finizola, A., Sortino, F., Lenat, J.F., Valenza, M., 2002. Fluid circulation at Stromboli volcano (Aeolian Islands, Italy) from self-potential and CO_2 surveys. Journal of Volcanology and Geothermal Research 116 (1–2), 1–18.

Finizola, A., Lenat, J.F., Macedo, O., Ramos, D., Thouret, J.C., Sortino, F., 2004. Fluid circulation and structural discontinuities inside Misti volcano (Peru) inferred from self-potential measurements. Journal of Volcanology and Geothermal Research 135 (4), 343–360.

Finizola, A., Aubert, M., Revil, A., Schütze, C., Sortino, F., 2009. Importance of structural history in the summit area of Stromboli during the 2002–2003 eruptive crisis inferred from temperature, soil CO_2, self-potential, and electrical resistivity tomography. Journal of Volcanology and Geothermal Research 183, 213–227. doi:10.1016/j.jvolgeores.2009.04.002.

Gibert, D., Pessel, M., 2001. Identification of sources of potential fields with the continuous wavelet transform: application to self-potential profiles. Geophysical Research Letters 28 (9), 1863–1866.

Grossmann, A., Morlet, J., 1984. Decomposition of Hardy functions into square integrable wavelets of constant shape. SIAM Journal on Mathematical Analysis 15 (4), 723–736.

Guichet, X., Zuddas, P., 2003. Effect of secondary minerals on electrokinetic phenomena during water–rock interaction. Geophysical Research Letters 30 (13), 1714. doi:10.1029/2003GL017480.

Harris, A.J.L., 2009. The pit-craters and pit-crater-filling lavas of Masaya volcano. Bulletin of Volcanology 71 (5), 541–558. doi:10.1007/s00445-008-0241-y.

Hase, H., Ishido, T., Takakura, S., Hashimoto, T., Sato, K., Tanaka, Y., 2003. Zeta potential measurement of volcanic rocks from Aso caldera. Geophysical Research Letters 30, 2210. doi:10.1029/2003GL018694.

Hase, H., Hashimoto, T., Sakanaka, S., Kanda, W., Tanaka, Y., 2005. Hydrothermal system beneath Aso volcano as inferred from self-potential mapping and resistivity structure. Journal of Volcanology and Geothermal Research 143, 259–277.

Hase, H., Hashimoto, T., Nishida, Y., Utsugi, M., Inoue, H., Saba, M., 2010. Hydrothermal system beneath Usu volcano inferred from self-potential observation and numerical simulation. Proc. World Geotherm. Congress, 2010, Bali, Indonesia.

Ishido, T., Mizutani, H., 1981. Experimental and theoretical basis of electrokinetic phenomena in rock–water systems and its applications to geophysics. Journal of Geophysical Research 86, 1763–1775.

Johnston, M.J.S., Byerlee, J.D., Lockner, D., 2001. Rapid fluid disruption: a source for self-potential anomalies on volcanoes. Journal of Geophysical Research 106, 4327–4335.

Join, J.-L., Folio, J.-L., Robineau, B., 2005. Aquifers and groundwater within active shield volcanoes. Evolution of conceptual models in the Piton de la Fournaise volcano. Journal of Volcanology and Geothermal Research 147, 187–201.

Jouniaux, L., Pozzy, J.P., 1995. Permeability dependence of streaming potential in rocks for various fluid conductivities. Geophysical Research Letters 22 (4), 485–488. doi:10.1029/94GL03307.

Jouniaux, L., Maineult, A., Naudet, V., Pessel, M., Sailhac, P., 2009. Review of self-potential methods in hydrogeophysics. Comptes Rendus Geoscience 341 (10-11), 928–936. doi:10.1016/j.crte.2009.08.008.

Legaz, A., Vandemeulebrouck, J., Revil, A., Kemna, A., Hurst, A.W., Reeves, R., 2009. A case study of resistivity and self-potential signatures of hydrothermal instabilities, Inferno Crater Lake, Waimangu, New Zealand. Geophysical Research Letters 36, L12306. doi:10.1029/2009GL037573.

Lénat, J.F., 2007. Retrieving self-potential anomalies in a complex volcanic environment: an SP/elevation gradient approach. Near Surface Geophysics 5 (3), 161–170.

Lewicki, J.L., Connor, C., St-Amand, K., Stix, J., Spinner, W., 2003. Self-potential, soil CO_2 flux, and temperature on Masaya volcano, Nicaragua. Geophysical Research Letters 30 (15), 1817. doi:10.1029/2003GL017731.

Maciejewski, A.J.H., 1998. Remote measurements of volcanic gases: Applications of Open-path Fourier transform infra-red spectroscopy (OP-FTIR) and Correlation spectroscopy (COSPEC), PhD thesis, The Open University, Department of Earth Sciences, UK, 348 pp.

MacNeil, R.E., Sanford, W.E., Connor, C.B., Sandberg, S.K., Diez, M., 2007. Investigation of the groundwater system at Masaya Caldera, Nicaragua, using transient

electromagnetics and numerical simulation. Journal of Volcanology and Geothermal Research 166 (3–4), 216–232.
Martin, R.S., Sawyer, G.M., Spampinato, L., Salerno, G.G., Ramirez, C., Ilyinskaya, E., Witt, M.L.I., Mather, T.A., Watson, I.M., Phillips, J.C., Oppenheimer, C., 2010. A total volatile inventory for Masaya Volcano, Nicaragua. Journal of Geophysical Research 115, B09215. doi:10.1029/2010JB007480.
Mauri, G., Williams-Jones, G., Saracco, G., 2010. Accurately determining the depths of hydrothermal systems by self-potential and Multi-scale wavelet tomography. Journal of Volcanology and Geothermal Research 191 (3–4), 233–244. doi:10.1016/j.jvolgeores.2010.02.004.
Mauri, G., Williams-Jones, G., Saracco, G., 2011. MWTmat— application of Multi-scale Wavelet Tomography on potential field. Computers & Geosciences 37, 1825–1835. doi:10.1016/j.jvolgeores.2010.02.004.
McBirney, A.R., 1956. The Nicaraguan Volcano Masaya and its Caldera. EOS, Transactions, American Geophysical Union 37 (1), 83–96.
Métaxian, J.-P., 1994. Étude Sismologique et Gravimétriqe d'un Volcan Actif: Dynamisme Interne et Structure de la Caldera Masaya. Université de Savoie, Nicaragua. 319 pp.
Métaxian, J.P., Lesage, P., Dorel, J., 1997. Permanent tremor of Masaya Volcano, Nicaragua: Wave field analysis and source location. Journal of Geophysical Research 102 (B10), 22529–22545.
Minsley, B.J., Sogade, J., Morgan, F.D., 2007. Three-dimensional source inversion of self-potential data. Journal of Geophysical Research 112, B02202. doi:10.1029/2006JB004262.
Moreau, F., Gilbert, D., Holschneider, M., Saracco, G., 1997. Wavelet analysis of potential fields. Inverse Problems 13, 165–178.
Moreau, F., Gilbert, D., Holschneider, M., Saracco, G., 1999. Identification of sources of potential fields with the continuous wavelet transform: Basic theory. Journal of Geophysical Research 104, 5003–5013.
Nadeau, P.A., Williams-Jones, G., 2009. Apparent downwind depletion of volcanic SO_2 flux: lessons from Masaya volcano, Nicaragua. Bulletin of Volcanology 71, 389–400. doi:10.1007/s00445-008-0251-9.
Pagli, C., Sigmundsson, F., Árnadóttir, T., Einarsson, P., Sturkell, E., 2006. Deflation of the Askja volcanic system: constraints on the deformation source from combined inversion of satellite radar interferograms and GPS measurements. Journal of Volcanology and Geothermal Research 152, 97–108. doi:10.1016/j.jvolgeores.2005.09.014.
Pearson, S.C.P., 2010, Diffuse degassing and the hydrothermal system at Masaya volcano, Nicaragua. Ph.D Thesis, University of South Florida, USA, paper 1736, 147 pp.
Pearson, S.C.P., Connor, C.B., Sanford, W.E., 2008. Rapid response of a hydrologic system to volcanic activity: Masaya volcano, Nicaragua. Geology 36 (12), 951–954.
Peterson, F.L., 1972. Water development on tropic volcanic islands type example: Hawaii. Ground Water 10, 18–23.
Poldini, E., 1939. Geophysical exploration by spontaneous polarization methods. Mining Magazine 60, 22–27.
Pribnow, D.F.C., Schütze, C., Hurter, S.J., Flechsig, C., Sass, J.H., 2003. Fluid flow in the resurgent dome of Long Valley Caldera: implications from thermal data and deep electrical sounding. Journal of Volcanology and Geothermal Research 127, 329–345. doi:10.1016/S0377-0273(03)00175-6.
Roche, O., van Wyk de Vries, B., Druitt, T.H., 2001. Sub-surface structures and collapse mechanisms of summit pit craters. Journal of Volcanology and Geothermal Research 105 (1-2), 1–18.
Rymer, H., van Wyk de Vries, B., Stix, J., Williams-Jones, G., 1998. Pit crater structure and processes governing persistent activity at Masaya Volcano, Nicaragua. Bulletin of Volcanology 59 (5), 345–355.
Sailhac, P., Marquis, G., 2001. Analytic potentials for the forward and inverse modeling of SP anomalies caused by subsurface fluid flow. Geophysical Research Letters 28 (9), 1851–1854.
Sailhac, P., Galdeano, A., Gilbert, D., Moreau, F., Delor, C., 2000. Identification of sources of potential fields with the continuous wavelet transform: complex wavelets and application to aeromagnetic profiles in French Guiana. Journal of Geophysical Research 105 (B8), 19455–19475.
Saracco, G., 1994. Propagation of transient waves through a stratified fluid medium: wavelet analysis of a nonasymptotic decomposition of the propagator. The Journal of the Acoustical Society of America 95 (3), 1191–1205.
Saracco, G., Labazuy, P., Moreau, F., 2004. Localization of self-potential sources in volcano-electric effect with complex continuous wavelet transform and electrical tomography methods for an active volcano. Geophysical Research Letters 31, L12610. doi:10.1029/2004GL019554.
Saracco, G., Moreau, F., Mathé, P.-E., Hermitte, D., Michel, J.-M., 2007. Multi-scale tomography of buried magnetic structures: its use in the localization and characterization of archeological structures. Geophysical Journal International 171 (1), 87–103.
Seaber, P.R., 1988. Hydrostratigraphic units. In: Back, W., Rosenshein, J.S., Seaber, P.R. (Eds.), The Geology of North America 0-2, Hydrogeology: Geol. Soc. Amer. pp. 9–14.
Shaw, A.M., Hilton, D.R., Fischer, T.P., Walker, J.A., Alvarado, G.E., 2003. Contrasting He-C relationships in Nicaragua and Costa Rica: insights into C cycling through subduction zones. Earth and Planetary Science Letters 214, 499–513. doi:10.1016/S0012- 821X(03), 00401-1.
Sorey, M.L., Suemnicht, G.A., Sturchio, N.C., Nordquist, G.A., 1991. New evidence on the hydrothermal system in Long Valley caldera, California, from wells, fluid sampling, electrical geophysics, and age determinations of hot-spring deposits. Journal of Volcanology and Geothermal Research 48, 229–263.
St-Amand, K., 1999. The distribution and origin of Radon, CO_2, and SO_2 gases and Multifractal behaviour of SO_2 at Masaya Volcano, Nicaragua, M.Sc. thesis, Université de Montreal, Canada, 270 pp.
Stoiber, R.E., Williams, S.N., Huebert, B.J., Sato, M., Matsuo, S., King, C., 1986. Sulfur and halogen gases at Masaya Caldera complex, Nicaragua; total flux and variations with time. Journal of Geophysical Research 91, 12215–12231. doi:10.1029/JB091iB12p12215.
Todesco, T., Rinaldi, A.P., Bonafede, M., 2010. Modeling of unrest signals in heterogeneous hydrothermal systems. Journal of Geophysical Research 115, B09213. doi:10.1029/2010JB007474.
Walker, J.A., Williams, S.N., 1986. Shallow magmatic processes beneath Masaya Caldera Complex, Nicaragua. Eos, Transactions, American Geophysical Union 67 (16), 411.
Walker, J.A., Williams, S.N., Kalamarides, R.I., Feigenson, M.D., 1993. Shallow open-system evolution of basaltic magma beneath a subduction zone volcano: the Masaya Caldera Complex, Nicaragua. Journal of Volcanology and Geothermal Research 56, 379–400.
Widén, B., Majdi, H., 2001. Soil CO_2 efflux and root respiration at three sites in a mixed pine and spruce forest: seasonal and diurnal variation. Canadian Journal of Forest Research 31, 786–796. doi:10.1139/cjfr-31-5-786.
Williams, S.N., 1983a. Plinian airfall deposits of basaltic composition. Geology 11, 211–214. doi:10.1130/0091-7613(1983) 11.
Williams, S.N., 1983b. Geology and eruptive mechanisms of Masaya Caldera complex, Nicaragua, PhD Thesis, Darthmouth College, Hanover, New Hampshire, USA, 169 pp.
Williams-Jones, G., Stix, J., Heiligmann, M., Charland, A., Sherwood Lollar, B., Garzón, V.G., Barquero, J., Fernandez, E., 2000. A model of diffuse degassing at three subduction-related volcanoes. Bulletin of Volcanology 62, 130–142.
Williams-Jones, G., Rymer, H., Rothery, D.A., 2003. Gravity changes and passive SO_2 degassing at the Masaya caldera complex, Nicaragua. Journal of Volcanology and Geothermal Research 123 (1–2), 136–160.
Zlotnicki, J., Nishida, Y., 2003. Review on morphological insights of self-potential anomalies on volcanoes. Surveys in Geophysics 24 (4), 291–338.
Zlotnicki, J., Michel, S., Annen, C., 1994. Self-potential anomalies and convective systems on La-Fournaise volcano (Réunion Island, France). Comptes Rendus de l'Académie des Sciences. Serie II, Sciences de la Terre 318 (10), 1325–1331.
Zlotnicki, J., Boudon, G., Viodé, J.P., Delarue, J.F., Mille, A., Bruère, F., 1998. Hydrothermal circulation beneath Mount Pelée inferred by self-potential surveying. Structural and tectonic implications. Journal of Volcanology and Geothermal Research 84 (1–2), 73–91.
Zlotnicki, J., Sasai, Y., Toutain, J.P., Villacorte, E., Harada, M., PHIVOLCS team, Yvetot, P., Fauquet, F., Bernard, A., 2009. Electromagnetic and geochemical methods applied to investigations of Hydrothermal/magmatic unrests: examples of Taal (Philippines) and Miyake-jima (Japan) volcanoes. Physics and Chemistry of the Earth 34, 394–408. doi:10.1016/j.pce.2008.09.01.